Department of Precision and Microsystems Engineering

Unit Cell with Sign-switching Poisson's Ratio for Adaptive Mechanical Metamaterials

Luca Lagemann

Report no : 2023.090
Coach : M. ten Wolde, Dr. ir. D. Farhadi
Professor : Dr. ir. D. Farhadi
Specialisation : Mechatronic System Design (MSD)
Type of report : Master's Thesis
Date : 13 October 2023

Unit Cell with Sign-switching Poisson's Ratio for Adaptive Mechanical Metamaterials

by

Luca Lagemann

to obtain the degree of Master of Science
at the Delft University of Technology,
to be defended publicly on Friday October 27, 2023 at 15:00

Student number:	5632986
Project duration:	September 2022 – October 2023
Thesis committee:	Dr. Ir. D. Farhadi, TU Delft, supervisor
	Ir. M. ten Wolde, TU Delft, supervisor
	Prof. Dr. Ir. J. L. Herder, TU Delft, chair

TU Delft Delft University of Technology

Preface

This master's thesis was written as part of the master Mechanical Engineering at the faculty of 3mE of the Technical University of Delft. Over the past year, I worked on a research project concerning the advancement of mechanical metamaterial. More specifically metamaterials with adaptive behaviour on the example of sign-switching Poisson's ratio. In the first part of the project, a thorough literature study was conducted. The findings of which are summarized in the literature survey report presented in Chapter 1. The second part of the project was devoted to bridge the identified knowledge gap. The results are presented in the format of a scientific publication in Chapter 2. Additional information on the methods and materials is presented in the supplementary materials in Chapter 3.

Contents

Chapter 1

Literature Survey: Towards Mechanical Metamaterials with Adaptive Poisson's Ratio

Towards Mechanical Metamaterials with Adaptive Poisson's Ratio

— Literature Survey —

Luca Lagemann
Delft University of Technology
MSc Mechanical Engineering, High-Tech Engineering, Mechatronic System Design
Delft, Netherlands
l.lagemann@student.tudelft.nl

***Abstract*—Mechanical metamaterials are architected materials with unique properties derived from their structure, rather than the material they consist of. Introducing different states into the material architecture allows to create of mechanical metamaterials with multiple effective properties that can be altered post-fabrication. A literature review is made on these so-called reprogrammable mechanical metamaterials with a focus on their state-switching strategies. Based on the findings, a new approach is suggested to create a reprogrammable mechanical metamaterial that can switch between positive and negative Poisson's ratio in response to the same external stimulus, by using information about its current state. This method enables adaptive property change, establishing the baseline for more advanced, multifunctional mechanical metamaterial.**

***Index Terms*—Adaptive, Poisson's ratio, Reprogrammable mechanical metamaterial, state-dependent**

I. Introduction

The mechanical properties of conventional materials are limited to a certain range. A scatter plot that depicts the relationship between two material properties of selected material classes, called Ashby-plot [1], is a good graphical representation that shows the limitations of these materials.

In the Ashby-plot shown in Fig. 1 the Young's Modulus is plotted against density for different commonly used material classes. These two properties are related to each other by a power law [2], which leaves a large area of inaccessible white-space [3]. The white space in the plot represents the range of material properties that have not yet been achieved or discovered. This results in the fact that desirable material properties such as low density and high stiffness, but also high strength & low density or high damping & high stiffness are mutually exclusive. This constrains the design space and practical applications of conventional materials.

It is therefore desirable to develop materials that could exhibit an arbitrary chosen set of mechanical and physical properties. Mechanical metamaterials aspire to do just that [4], [5].

Mechanical metamaterials (MM) are architected materials composed of building blocks (unit cells) and exhibit certain unusual properties. Rather than just combining different materials, as in composite materials, MM derive their behaviour

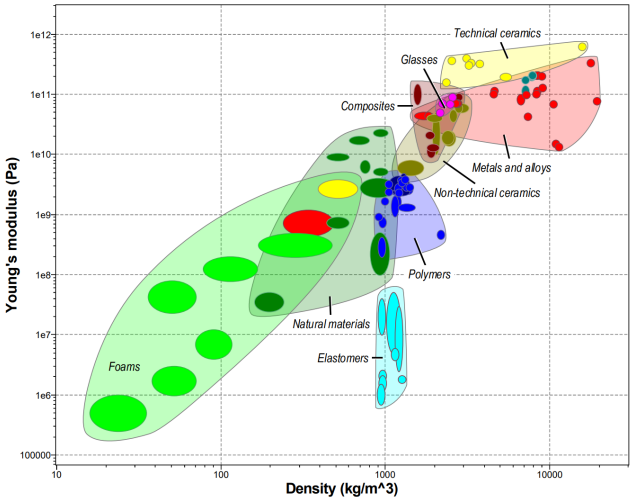

Fig. 1. Typical material selection chart (Ashby-plot) comparing Young's Modulus and density of different material classes. This plot was generated using the ANSYS software Granta EduPack 2022 R1.

from the rationally designed structure of its unit cells, leading to properties that can go beyond (="meta", Greek) those of its constituent materials.

The concept of metamaterials originated in the field of electromagnetism in the late 1990s, where the unusual property of negative refractive index has led to the development of a perfect lens [6] and invisible cloak [7]. Over time the idea behind metamaterials was extended to other fields, such as acoustic, mechanics, and thermodynamics [8].

Pushing the boundaries of accessible material behaviour has been one of the driving forces of the metamaterials field [9]. Furthermore, rapid development in computer-aided design (forward as well as inverse design techniques) and manufacturing technologies like 3D printing and micromachining has opened up new possibilities to rationally design the materials microstructure and apply engineering and architectural principles at the material scale.

Figure 2 visualizes how the tessellation of these architected unit cells leads to the creation of materials with certain effective properties (d. to f.), compared to natural materials (a. to c.).

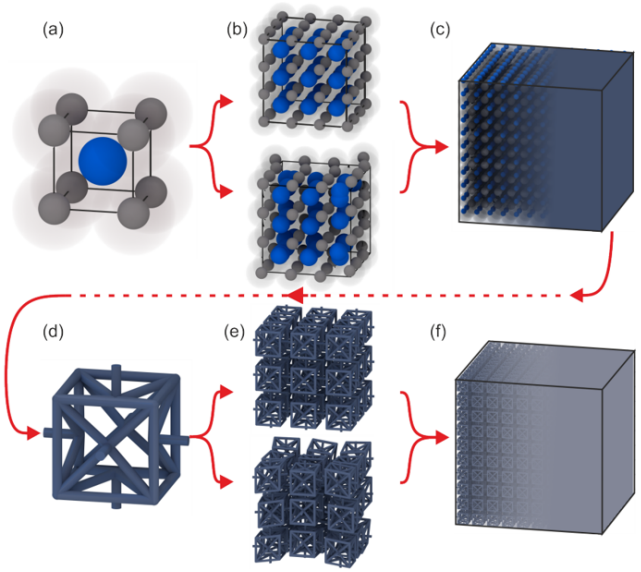

Fig. 2. Natural material and its atomic structure (a) to (c) compared to a mechanical metamaterial composed of rationally designed unit cells (d) to (f) [9].

The unit cells of mechanical metamaterials, sometimes also called meta-atoms, deform, rotate, buckle, fold and snap in response to mechanical forces and are designed such that adjacent building blocks can act together to yield a desired collective behaviour. Carefully designed architectures can be used to achieve any combination of linear elastic coefficients that is not forbidden by thermodynamics [10].

Well-known examples are auxetic materials, which exhibit a negative Poisson's ratio. Most natural materials (with a few exceptions [11]) have a positive poisson's ration. This means they contract laterally under axial tension. Metamaterials with a specific structure, as shown in Fig. 3, on the other hand, expand laterally under axial tension, resulting in a negative Poisson's ratio.

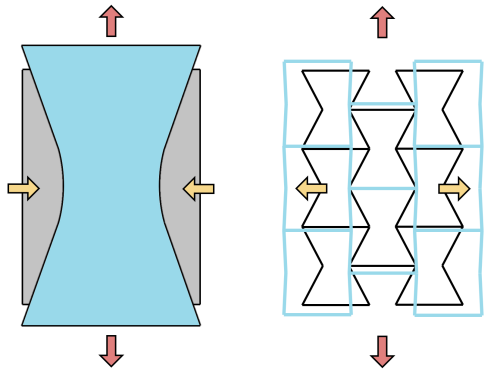

Fig. 3. Normal material and rationally designed metamaterial under axial tension experience different lateral displacements. Left: normal material with positive Poisson's ratio. Right: rationally designed metamaterial with negative Poisson's ratio.

Other examples of negative parameter metamaterials are those which can exhibit negative compressibility [12], [13], negative stiffness, which is often associated with buckling or snap through behaviour [14], and negative thermal expansion coefficient [15], [16].

Furthermore, MM have led to the development of penta-mode materials, which behave similarly to a fluid due to its very large bulk modulus and small shear modulus [17]. Bückmann et al. [18] have used penta-mode metamaterials to create a "unfeelability cloak". It's counterpart, dilational metamaterials, have an extremely high bulk modulus compared to the shear modulus, leading to an auxetic material behavior with the special effect that the shape of the material remains the same regardless of how much deformation they undergo. In other words, dilational materials are merely scaled as a result of deformation [19].

Ultra-property MM are able to possess two or more of the following properties: high stiffness, high strength, high toughness, and low mass density [4]. Meza et al. [20] demonstrated ultra-strong and ultra-light metamaterials. An example for high stiffness and low density was given by Zheng et al. [21].

These are just a few examples and the field of application of mechanical metamaterials is vast. In all cases, subtle changes in the geometry of the disordered networks lead to qualitatively different deformations and elastic properties, which illustrates that the relation between the architecture and collective properties is rich and complex [10].

II. Problem Statement

The unique characteristics of mechanical metamaterials are undoubtedly useful and can enhance the performance of systems or even accomplish tasks that were not possible before. However, this comes with a limitation: these MM are designed to exhibit a specific behaviour; After fabrication, this behaviour can not be modified. In other words, their functionality is limited to what has been programmed into the material structure by its rational design. The question therefore arises if and how MM can be created so that they can be reprogrammed to change their material behaviour even after fabrication.

Reprogrammable mechanical metamaterials represent a significant advancement in the field of metamaterials, enabling the rational design of MM with multiple, tailored properties. While traditional MM have made it possible to access the unexplored white space of the Ashby-plot through their unique mechanical properties, reprogrammable MM have the potential to access multiple areas in the white space by altering their properties post-fabrication. Crucial for the development of reprogrammable MM is the ability to control and reconfigure the microstructure of the metamaterial as it determines its mechanical properties. Figure 4 illustrates the ability to reprogram the property of a material after fabrication. Green and red indicate two different states of the unit cell microstructure, with distinct mechanical properties. Depending on the architecture, the state can be switched collectively or even on individual unit cell level, leading to a larger number of possible configurations.

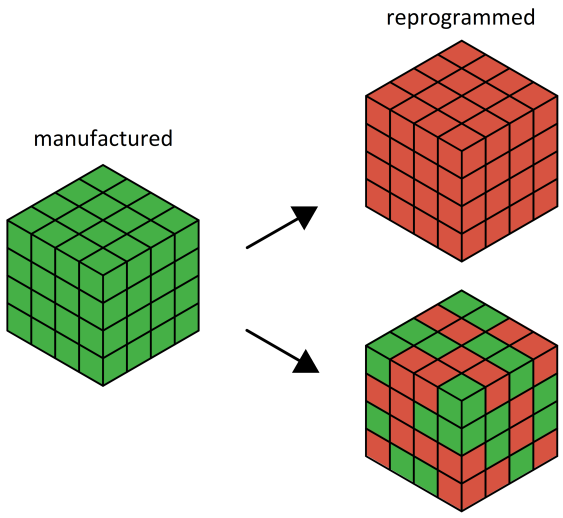

Fig. 4. Reprogrammable mechanical metamaterial. Left: material consisting of individual unit cells, manufactured in one state. Right: post-fabrication reprogrammed metamaterial.

The ability to control and adjust the material structure and therefore its property for specific applications or environments allows for greater versatility and adaptability, making reprogrammable MM more suitable for a wide range of applications, such as soft robotics, aerospace, and biomedical engineering. Therefore, the development of reprogrammable MM has emerged as an urgent and promising area of research, with significant potential for solving real-world engineering challenges. The following section provides an overview of different applications and design strategies of reprogrammable mechanical metamaterials by summarizing the current state of the art in this field.

III. Literature Research

This section will provide an insight into the conducted literature review on reprogrammable mechanical metamaterials by first outlining the research methodology (section III-A). After that the current state of the art is presented (section III-B) and then further elaborated through a classification of the findings (section III-C).

A. Research Methodology

To conduct the research on the current state of the art in the field of reprogrammable mechanical metamaterials, a thorough examination of existing literature was performed. This involved starting with review papers to obtain a general understanding and overview of the field, followed by generating a list of keywords to locate relevant papers (shown on the left of Fig. 5). From there, seed papers were identified and their citation network was examined to find related papers. The graph on the right of Fig. 5 shows the citation network of a specific set of seed papers. Throughout the research process, different combinations of specific works and review papers were investigated. Additionally, the works of influential authors to gain a more complete understanding of their contributions to the field. All of the collected information was then gathered and compared from different angles to derive a research question.

reprogrammable		mechanical metamaterial
programmable		metamaterial
adaptive		matter
adaptable		unitcell
tunable		mechanical bit
multifunctional		m-bit
functional	AND	
adjustable		
bistable		
multistable		
multimodal		
configurable		
reconfigurable		

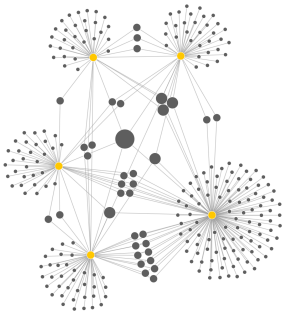

Fig. 5. Literature research tools. Left: List of research keywords. Right: Citation network and connecting papers of a few seed-papers using Citation Gecko [22].

B. State of the Art

Several metamaterials, that can alter their mechanical property after fabrication in a reprogrammable manner, have emerged. One significant contribution, that could be considered a landmark paper for the terminology ”reprogrammable mechanical metamaterial” is by Chen et al. [23]. In this paper reprogrammability of a material property was demonstrated analogous to that of digital devices, in which each unit can be written to or read from in real-time, as required. This was done by using physical binary unit cells (m-bits), that can be independently and reversibly switched between two stable states. Tessellation of these unit cells results in a reprogrammable metamaterial with a stiffness and strength that can range over an order of magnitude. A bistable dome is used as a state element that is linked to two distinct stiffness states which can be switched by magnetic actuation and physical loading is used to read the material state. [23]. Ma et al. [24] used a similar approach to design a voxel-based metamaterial with different poisson’s ration and stiffness states to simultaneously reprogram mechanical properties and shape-morphing [24]. Interestingly this example investigated loading conditions where the unit cells were tested in parallel as well as in series, which is relevant when going from 2D to 3D metamaterial tessellation.

In general, any kind of structural transformation of architected materials achieved by mechanical or environmental stimuli can be viewed as an analogy to the phase transformation of crystalline materials [25]. If this phase transition is reversible, the so-called phase transforming metamaterials can be considered reprogrammable. Restrepo et al. [26] extended the notion of phase transformation to periodic cellular materials by implementing unit cells with multiple stable configurations into the material. Each stable configuration of the unit cell corresponds to a stable phase, and transitions between these phases are regarded as phase transformations of the cellular material. The presented metamaterial in this paper shows hysteresis in loading and unloading, making it attractive for energy absorption applications. Other examples have extended this concept to 3D through the use of multistable perforated shellular motifs [27]. Besides the benefit

of enhanced energy damping, the ability of the material to have multiple stable configurations could be used to create a reprogrammable metamaterial, where each phase of the material offers a different mechanical behaviour.

Similarly Florijn et al. [28] demonstrated that the pattern transition of a biholar sheet under compression is determined and can be programmed by lateral confinement. Inhomogenous confinement even leads to giant hysteresis and multistability, which can be exploited for reprogrammable metamaterials whos functionality can be altered by changing the boundary conditions. Three interesting observations need to be pointed out: the effect of hysteresis, multistablity thorugh frustration, and the transition wave through the material while it switches from one state to the other. Hecke et al. continued to explore the effect of hysteresis and sequential state transition [29] and very recently realized irreversible metamaterials that can count mechanical driving cycles and store the result into easily interpretable internal states [30]. This highlights the potential of multistable mechanical metamaterial for information processing, which has more and more been considered to be treated as a material property [31]. The transition front that is moving through the material when it is undergoing phases of transition has been used for propagating mechanical signals in metamaterials [32], [33], which can be useful to control or transport signals in harsh environments. These examples also show that a local actuation can lead to a global state change of the metamaterial, which can be interesting for reprogrammable MM. One problem though is the energy dissipation that occurs during the snapping of bistable elements. This makes returning to the initial state of the metamaterial challenging. Jin et al. [34] extended the idea of transition waves to 2D and demonstrated that the direction, shape and velocity of the transition wave can be precisely controlled by spatially tailoring the underlying periodic network architecture through local defects for example. The demonstrated use case for shape morphing and reconfigurable devises could be enhanced if one could reprogram the location of such defects, giving rise to reprogrammable shape morphing. Also interesting to note is that the unit cell by itself is monostable, but when tessellated becomes bistable due to the suppression of rotational rigid-body modes by the network.

Frustration and interaction between bistable unit cells is an effective design strategy for reprogrammable MM. For instance, it was shown that an elastomeric sheet with bistable domes can exhibit distinct three-dimensional conformations based on the order of dome inversion not just the specific combination of inverted domes [35], [36]. In contrast to other multistable metamaterial architectures with equal units, this work shows distinct spatiotemporal deformation sequences allowing to access specific global states. Metamaterials underlying this non-abelian response are another direction of ongoing research [37]. In [38] a combinatorial strategy for the design of aperiodic, yet frustration-free, mechanical metamaterials that exhibit spatially textured functionalities, was presented. By including vacancies or defects, controlled frustration can be introduced to obtain multistability, memory and reprogrammability. Mei et al. [39] use bistable constraint beams and their interaction on snap-through to create a mechanical metamaterial with that can perform basic logical functions. Actuated by electromagnets individual units can be reprogrammed to achive different logic functions.

As mentioned before, some examples are not directly associated with the term reprogrammable mechanical metamaterials as such. But their ability to switch between different states or phases still make them relevant examples. Clever structural design can take care of attaching a mechanical property to the state change. An example of a metamaterial that can change its mechanical property upon state change can be found in the work of Zadpoor et al. [40]. In this case, the metamaterial enters either auxetic or conventional behaviour, depending on the speed of actuation. This was achieved by laterally attaching two beams of elastic materials with different strain-rates. Thereby the axial loading rate decides rather the so-called bi-beam buckles to the left or right, leading to different mechanical behaviours. Another example of how strain mismatch is used as a construction principle of mechanical metamaterials was shown by [41] where materials of different thermal expansion coefficients are used to create a metamaterial with sign-switching Poisson's ratio. MM with the ability to toggle between negative and positive poisson's ratio have also been demonstrated by making use of compliant members and self-contacting hard stops, which engage or disengage under loading. Leading to the development of mechanical metamaterial with different Poisson's ratio signs under tension and compression [42] and even sign-switching Poisson's ratio under unidirectional loading [43]. A significant distinction and potential disadvantage of these examples compared to the previous once is that they are volatile, which means that these materials need a constant energy supply to remain in one of their states. An interesting middle ground is to use metastable behaviour, where the material returns to its initial state after a certain time. Implementing geometric nonlinearity (snap through) as a hierarchical level into the unit cell design resulted in a metamaterial with time-dependent shape memory, which has advantages for applications in the field of medicine [44].

Most examples so far make use of nonlinear force-deflection behaviour in form of beam-like buckling or snap-through. Another strategy which has been widely used are origami-inspired mechanism that can fold along predefined creases. Exploring the competition between bending and hinging energies allows the design of multistable and reprogrammable materials [10], [45]. Each unit cell within a 2D tessellation of the Miura-ori fold for example is bistable and by switching (popping through) individual cells, the compressive modulus of the overall structure can be rationally and reversibly tuned [46]. Another origami structure that experiences bistability is the Kresling fold. The states are achieved by either applying an axial force or torque. The Kresling pattern has been used to create mechanical metamaterials with tunable stiffness and memory operation [47], [48]. Kirigami-inspired metamaterials are produced by introducing arrays of cuts into thin sheets of a material, which allows for extremely large strains and shape changes [10]. Yang et al. [49] used Kirigami to create a unit cell that can switch between four patterns with different acoustic properties. Two-dimensional tessellation of this unit cell

leads to a reprogrammable MM with an exponentially large number of configurations that can act as a wave filter, guide, lens or cloak. A mechanical metamaterial consisting of modular origami-based polyhedra structures was demonstrated by Overvelde et al. [50]. The structure can be actively deformed into numerous specific shapes through embedded pneumatic actuation, leading to tunable shape, volume, and stiffness. Since the proposed structure has only one energy minima it requires constant actuation to maintain a configuration than its initial one. Iniguez-Rabago et al. [51] introduced a strategy to overcome this volatility by exploring the complex energy landscape of 3D prismatic structures and identifying additional stable configurations of the structure. Through this multistable behavior, reprogrammable metamaterials from 3D prismatic building blocks are a possible candidate for applications like reconfigurable acoustic waveguides, microelectronic mechanical systems and energy storage systems. Another mechanism-based mechanical metamaterial was proposed by Liu et al. [52]. Here the topological transformation of the Wohlhart polyhedron is exploited to construct a reprogrammable MM with Poisson's ratio ranging from negative infinity to positive infinity. Due to kinematic bifurcation, the polyhedron can exhibit negative, positive, and zero Poisson's ratio depending on its kinematic pathway.

Overall these examples point out that there is an increasing interest in the relatively new field of reprogrammable mechanical metamaterials. A wide range of design strategies have been explored to serve different fields of applications. Many examples make use of buckling or snapping beams, others rely on the complex energy landscape of mechanism-based structures, including origami and kirigami. Some exploit the interaction between unit cells to perform logic functions or allow a local actuation to cause a propagating state transition through the metamaterial while others use independent unit cells that can be switched individually to drastically increase the number of possible global configurations. While earlier examples often show one- or two-dimensional realizations, the state of the art has reached 3D metamaterials for most applications. It is clear that a lot of research has been conducted on achieving multistability in metamaterial structures and how this can be utilized to create reprogrammable MM. But not so much attention has been paid to the actual cause of the state change. Most examples from literature simply use or refer to stimuli-responsive or smart materials for this matter. These materials deform as a response based on external environmental stimuli such as magnetic, electric, light, or thermal fields [25] and thereby cause the metamaterial to switch states. The actual relation between input and output, or in other words the reason for a metamaterial to change its state seams less explored. Therefore, in the following section, state transition strategies will be further analyzed through a classification based on the state of the art.

C. Literature Classification (state transition)

The goal of this classification is to identify similarities and differences or even gaps where improvements can be made. To create an abstract and simplified visual representation of the different state transition strategies found in the state of the art of reprogrammable MM, inspiration was taken from graph theory and state diagrams. These graphs show the various states the metamaterial can be in, and the trigger that causes it to transition form one state to another. The states, which in the sense of reprogrammable MM represent the different configurations of the material that can have distinct mechanical properties, are indicated by circles with capital letters. State transitions of the material are symbolized by arrows between states, which are labeled by Arabic numbers that indicate the specific input that causes the transition.

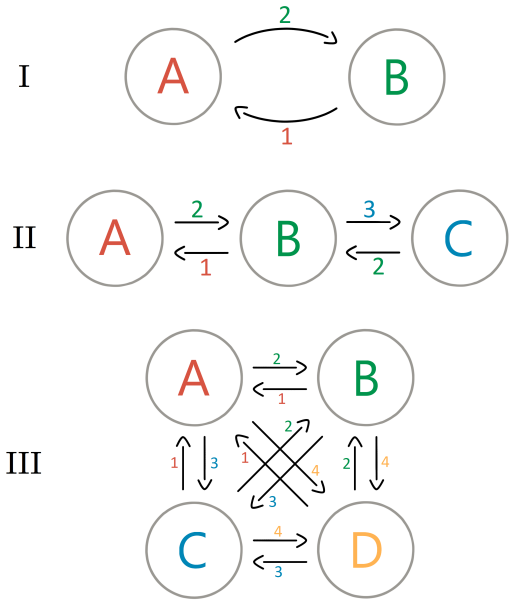

Fig. 6. Classification of different state transition strategies. Circles with letters represent the different states of the metamaterial and the arrows together with the number label represent the distinct input required to access the respective state. I: globally reprogrammable. II: sequentially reprogrammable. III: locally reprogrammable.

As shown in Fig. 6, the state transition strategies identified in the state of the art can be divided into three different classes. An overview that also includes literature examples for each class can be found in Appendix A.

The first group in this classification can be considered as "globally reprogrammable". Examples following this strategy have two states and a specific trigger causes a state transition over the entire structure, simultaneously. This group includes metamaterials used for signal transition [32], [33], transition wave propagation [34], and systems that can switch between different shapes [51]. In these cases, a local actuation can cause a global state change. This attribute comes at the cost that returning to the initial state often requires more energy and effort. Furthermore, the number of global states is coupled to the number of states per unit cell. The structure of bistable unit cell has two global configurations.

The second class is referred to as "sequentially reprogrammable". In this case, the metamaterial can have multiple states and their transition occurs in a predefined sequence. Even though the corresponding state diagram in Fig. 6 II shows

three states, the number of states is not limited to this. A set of stimuli needs to be applied to the material in a specific order to achieve the desired state. This class includes volatile reprogrammable MM [40], [43] where the centre state is a ground state, as well as non-volatile reprogrammable MM with sequential phase transition [26], [28], [27]. Although increasing the number of states is generally beneficial, in these cases increasing the number of states also compromises the functionality per state. Since the total deformations are stress-limited and each state is linked to its own range of deformation, the effective range per state decreases with an increasing number of states.

Lastly, the class of "individually reprogrammable" metamaterials, includes those which allow unit cells to switch individually and independently [23], [24], [49], resulting in a large number of possible configurations. Again the state diagram (Fig. 6 III) is an oversimplified representation, which only shows four states. This could be achieved by a metamaterial consisting of two individual bistable unit cells, resulting in 2^2 possible configurations. Without discarding equivalent states due to symmetry, the number of possible states goes by number of states per unit cell to the power of number of cells. Extremely large numbers of possible states can be extremely useful. For example, looking back at the potential of reprogrammable MM to have different locations in the Ashby-plot. Increasing the number of material states increases the number of locations in the Ashby-plot. At this point, controlling all possible configurations by individually changing the states of unit cells becomes a challenge.

Despite their different functionality the three classes of state transition strategies share a significant characteristic: Each state has its own distinct input. This means that a specific state can only be accessed by a specific input and vice-versa. Consequently, n number of states requires n number of distinct inputs. In mathematics, a bijective function is a one-to-one correspondence between the elements of two sets, such that each element of one set is inversely paired with exactly one element of the other set. This same behaviour can be identified here for the inputs and states. An interesting and unexplored research direction is that of a state transition strategy without bijection between input and state.

IV. Knowledge Gap

A promising approach to break the bijective link between input and state is to move from input-dependent switching to state-dependent switching, by making use of the internal information of the current state. This way the next state of the material is no longer decided by the external stimulus (input) but rather the current state. This creates the opportunity to switch between two states under the same external stimulus as shown in Fig. 7.

Applying state-dependent switching to the field of reprogrammable MM is a novel approach which could open up new possibilities and advanced functionalities.

First of all the number of inputs is no longer required to equal the number of states, which leads to less controlled input parameters. For example: a metamaterial with two states

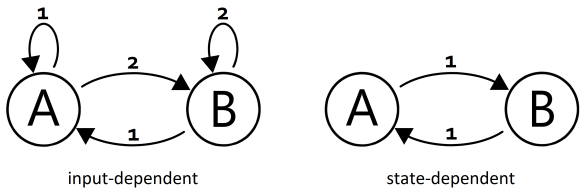

Fig. 7. State transition diagrams. States are indicated by a letter in a circle and the arrows represent the input. Left: input-dependent state change. Right: state-dependent state change.

previously required two distinct inputs (one for each state). With state-dependent switching it is now possible to switch between the two states using one external input (see Fig. 7). To this point the word *input* has been used for the external stimulus that is required to change the state of the metamaterial. Once a material property is attached to the state, another input is required to test or exercise this property. Taking the example of a mechanical metamaterial with reprogrammable stiffness. One input is responsible for changing the stiffness state, which from now on is considered the textitwrite-input. In use, the metamaterial is subjected to another input to exercise its property. In the case of stiffness, this can be a mechanical load like force or displacement. This input will be referred to as textitread-input. Now given the ability to avoid the bijection of state and input through input-dependent switching, generates new opportunities to combine read- and write-input by using a threshold as a switching point. Integrating read and write into one physical input has been done before in some examples from literature [40], [43] though with the significant disadvantage that the direct link between input and state compromises the functionality, as mentioned before. Using a threshold and breaking the bijection of inputs and states could resolve this problem so that all states can exercise the same deformation regime. An exemplary figure of this effect is shown in Appendix B.

Strikingly, breaking the link between input and state allows to move from responsive behaviour to adaptive behaviour [53], making the next step in the direction of intelligent materials [54]. Figure 8 showcases the ability of adaptive property change in a simplistic manner. The presented reprogrammable MM consists of four individually bistable unit cells. The two different states, indicated as green and red, are associated with distinct mechanical properties.

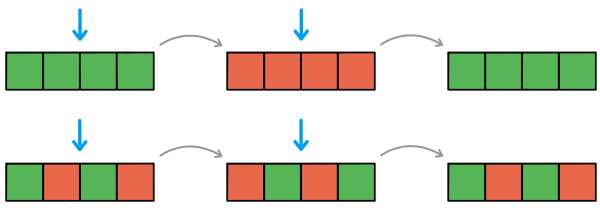

Fig. 8. Adaptive property change illustrated by a mechanical metamaterial consisting of four bistable unit cells. Two distinct unit cell states are highlighted by the two colours green and red. The blue arrow represents the external input and the grey arrows indicate the next evolution of the metamaterial after the input has been applied.

The top row of the figure points out the ability to switch

between two metamaterial states using the same input, as described before. Under different circumstances, the metamaterial may have a different initial configuration. Applying the same input as before now leads to a totally new configuration and therefore material property. This adaptive property change is unprecedented in the field of mechanical metamaterials and may lead to new designs with advanced functionalities that go beyond the user-guided and responsive reprogrammability of mechanical metamaterial properties. For additional information on potential future applications and research trends, refer to Appendix C.

V. Research Question

After analyzing the state transition strategies from the state of the art, identifying the gap of state-dependent switching and envisioning its potential for adaptive property change, the applicability still remains to be demonstrated. Therefore the research question is defined as:

> **How can state-dependent switching be utilized to create a reprogrammable mechanical metamaterial with adaptive property change?**

This rather general question can be split into more specific sub-questions which may be answered individually:

- How can state-dependent switching be achieved in a mechanical system?
- Which mechanical property and how can it be associated to the state change?
- What kind of tessellation can be used to create a mechanical metamaterial?

VI. Project Goal

This section describes how the three sub-questions will be solved throughout the project in order to derive a solution that can answer the research question. First, different strategies for state-dependent switching are investigated and compared to find the most promising approach. Second, a unit cell design will be derived that incorporates the state-dependent switching and associates a mechanical property which changes with the geometrical change of the cell upon state transition. The third and last step covers the tessellation of the unit cell to create a mechanical metamaterial.

These steps are executed under a few constraints to ensure that the solution is feasible, functional and in line with the research question: The system shall be non-volatile and (down-)scalable. The read- and write-input shall be combined, whereas the input is mechanical, such as force or displacement, and the output is a function of the current state and the input.

1. State-dependent switching

Linkages or compliant mechanisms that utilize state-dependent switching can switch between multiple states under the same input. In literature, these mechanisms are also referred to as ”push on - push off”, ”single input - double output”, or ”single actuator bistable” -mechanisms. The different examples found in the literature can be grouped by their strategy.

The first group follows the latch-lock principle, where under the first event of actuation, the mechanism latches and causes other structural components to lock into place, which represents the second state. With the subsequent actuation, the mechanism is unlatched due to its current configuration, causing the system to return to its initial state. The mechanism commonly used in pens follows the same principle. Two dimensional, scalable designs of this switching mechanism have been proposed for use in MEMS devices [55], [56], [57].

A differnt approach that makes use of bistable beams as the state element, has been proposed by Huang et al. [58] [59]. In these examples, both states are basically actuated at the same time and depending on the current state, the actuation is guided such that it causes a state transition to the other state.

Recently, another mechanism has been reported, which consists of a buckling input beam that is at bifurcation, a nonlinear spring, and a bistable beam as the state element [60]. The nonlinear spring connects the input beam and the state element. It reads the state of the state element and displaces the input beam at bifurcation such that its buckling path changes with the state. Upon actuation, the input beam is axially compressed and is buckling-induced lateral displacement causes the system to change states once a certain displacement threshold is reached. Figure 9 shows a sketch of this state-dependent switching mechanism in both of its states.

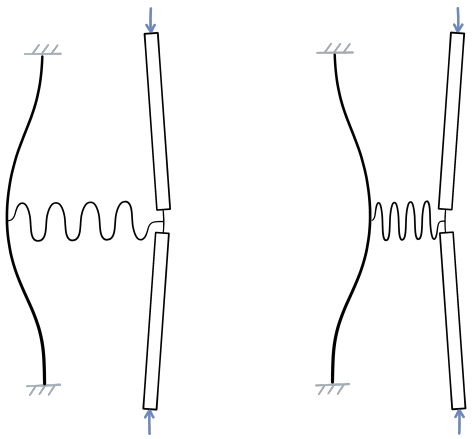

Fig. 9. State-dependent switching concept and its two states. The left buckled beam represents the state element and the columns on the right the input beam. Both elements are connected by a central non-linear spring.

The advantage of this concept compared to the previous once is that it is robust, contactless and it has certain advantages in its geometric change. Due to the changing buckling direction of the input beam, both the state element and input beam experience a significant geometric change upon state transition, which can be useful for associating a mechanical property to the system. Therefore this concept was chosen as the state-dependent switching strategy for this project.

2. Unitcell & property

The components of the state-dependent switching concept described above were used as a baseline to design a unit cell and associate a mechanical property to the geometric change. Taking two of these mechanisms back-to-back and connecting

the upper endpoints and lower endpoints of both mechanisms respectively, leads to a square shape unit cell. The resulting unit cell is shown in Fig. 10 for both states. Due to the previously described working principle of this mechanism, the input beams (marked in red) buckle outward in the first state and inward in the second state. This displacement behaviour lends itself well to the property of sign-switching Poisson's ratio. The concept of which has been introduced earlier in this report. The Poisson's ratio of a material is defined by the following formula:

$$\nu = -\frac{\varepsilon_{\text{lat}}}{\varepsilon_{\text{long}}} = -\frac{\text{lateral strain}}{\text{longitudinal strain}}$$

It is obvious that the exact value depends on the dimensions of the unit cell and varies with the inclined angle of the input beam. Liu et al. [61] reported feasible Poisson's ratio values for this kind of structure that range from -3.3 to 3.3.

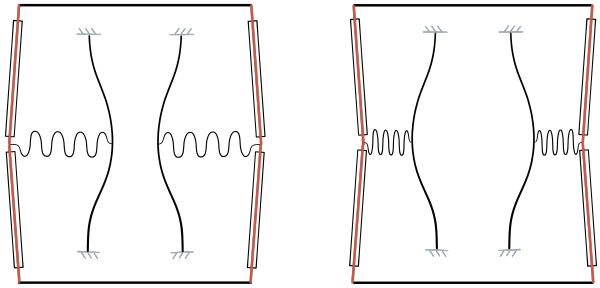

Fig. 10. Two states of the unit cell design with sign-switching Poisson's ratio. The input beams are highlighted in red. Left: input beam buckling outward, resulting in positive Poisson's ratio behaviour. Right: input beam buckling inwards, resulting in negative Poisson's ratio behaviour.

3. Tessellation

To create a metamaterial, the described unit cell will be tessellated in a honeycomb-like structure. Figure 11 shows an example of this tiling in a 5x3 grid. Again, the read lines indicate the input beams that either buckle inward or outward, depending on the state of the unit cells. The dotted lines show the circumference of the undeformed metamaterial, highlighting the two different Poisson's ratios of the two states.

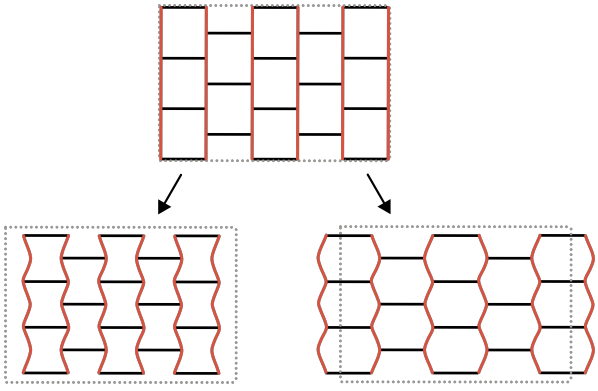

Fig. 11. Tessellated unit cell structure. Top: undeformed. Bottom left: deformed in negative Poisson's ratio state. Bottom right: deformed in positive Poisson's ratio state.

VII. Feasibility

This section summarizes some actions and tasks that have already been done or investigated in order to ensure the practicability of the proposed project and resolve potential road blockers.

A crucial building block of the proposed design is the state-dependent switching mechanism described in the previous section. To verify its desired functionality, the working principle was analysed in an ANSYS model provided by the author and designer of the mechanism ten Wolde et al. [60]. The FEM model was also used to perform some exploratory analysis of the underlying parameter space to modify the switching behaviour of the mechanism.

For the proposed honeycomb tessellation to be a viable option, it is necessary that it allows the grid to deform homogeneously under load, so that all unit cells experience the same amount of stresses and strains. If this was not the case, it would not be possible to change the states of all unit cells. For this purpose, an initial FEM analysis was performed on a hexagon sample with notch flexures as hinges. Under in-plane compression, the model showed that the stresses in the flexures are the same across the whole grid, which validates the feasibility of the hexagon tessellation. An image of the performed FEM analysis can be found in Appendix D.

In order to check the feasibility of fabrication, a few test prints using FDM (fused deposition modelling) 3D printing and PLA material were made. Some of the samples fractured under snap through, likely due to its relatively high flexural modulus (3-5GPa [62], [63]). An image of PLA test prints can be found in Appendix E. Besides being too brittle, PLA also showed a slow and continuous plastic deformation of the material over extended periods under load. This phenomenon known as creep is undesirable especially for bistable elements since it influences the energy landscape and therefore the switching operation. Furthermore, the resolution and inconsistency of FDM printers could lead to higher deviations between as-designed and as-manufactured functionality. Using stereolithography (SLA 3D printing) seams to be a promising alternative due to its much higher printing resolution and accuracy. The available SLA printer for this project is a Form 3+ from Formlabs. A study of the available materials and their properties led to the decision to use Tough 2000 [64]. This material has a high ratio between flexural stength and flexural mudulus, which is important for compliant mechanisms. The flexural strength sets the limit in terms of stresses, so it should be as high as possible. The flexural modulus relates to stress and strain under deformation and describes the tendency of the material to resist bending. In other words, the flexural modulus of the material defines the slope of its elastic deformation in the stress-strain plot. For compliant mechanisms, it is desired to have a low flexureal modulus (small slope) so that the displacement range until the stress limit is maximized. PU 1000, which showed an even higher flexural strength-to-modulus ratio, requires extensive time and effort for post-processing. Therefore it's use is neglected for now but remains a backup option.

In order to test the fabricated metamaterial or individual

elements, a PI (Physik Instrumente) test setup from the university's PME lab can be used. This test setup was designed to measure and record the force-displacement relationship of compliant mechanisms.

VIII. Planning

This section outlines the methodology and steps that are planned to execute the research project.

At first, a kinematic model of the unit cell will be created that incorporates the state-dependent switching mechanism. This model will then be used to determine design parameters like stiffnesses and dimensions that lead to a desired behaviour. The primary goal is to be able to precisely define the threshold that causes state transition and match their values for both switching situations (from negative to positive Poisson's ratio and vice versa). Furthermore, the unit cell should preferably be able to experience as much displacement as possible before switching so that its Poisson's ratio can be displayed over a larger range of motion. Though, this is expected to be constrained by the primary goal. The model is expected to provide information about these functional limits of the mechanism.

Simultaneously, critical elements such as bistable beams and flexures will be fabricated via SLA 3D printing and tested. Thereby the material parameters are verified and deviations can be taken into account at an early stage of the design phase. This process may include multiple iterations.

Once a set of parameters with desirable performance is found, an ANSYS APDL model will be created. After cross-validation of kinematic model and simulation model, a complete unit cell will be fabricated and tested as well. If its functionality is guaranteed and matches the models, the next steps can be taken.

Next, a model of the tessellated structure will be created. With this model, the switching behaviour of the full metamaterial structure is analysed. Additionally, a variety of scenarios such as different initial configurations of unit cells and special boundary conditions can be tested.

Finally, the full structure will be fabricated, tested and compared to the simulation model.

A timeline of the proposed actions can be found in Appendix F.

IX. Conclusion

Mechanical metamaterials (MM) offer a promising avenue for achieving tailored properties that are not easily accessible with conventional materials. This is primarily due to their unique architectural designs, rather than the constituent materials they are made of. Traditionally, MMs were designed to exhibit a particular set of behaviours, which once fabricated, could not be modified. However, the emerging field of reprogrammable mechanical metamaterials seeks to transcend this limitation by allowing these materials to modify their behaviour post-fabrication.

A critical observation from the literature is that the conventional approach to state transition in MMs is based on a bijective relationship between inputs and states. This method requires distinct inputs for distinct states, which requires complex actuation strategies and restricts the metamaterial's functionality. An unexplored avenue is state-dependent switching, where the current state determines the next state, rather than the external stimulus. This would enable the metamaterial to switch between various states using the same external input.

Transitioning from the conventional input-dependent switching to the state-dependent model could pave the way for MMs that are not just responsive but adaptive. Such adaptability could drastically broaden the potential applications of MMs and pave the way for more intelligent mechanical metamaterials by leaving part of the decision-making to the material itself. Future research in this direction holds the promise to introduce a paradigm shift in the field of reprogrammable mechanical metamaterial with advanced functionality and applicability.

In light of the findings from the literature review, we propose the use of internal instability in the form of bistable elements to allow state-dependent switching. This approach will be integrated into a contactless and tessellatable unit cell design, facilitating the distinct states of negative and positive Poisson's ratio.

References

[1] M. Ashby, *Materials Selection in Mechanical Design*. Elsevier Science, fifth ed., 2016.

[2] L. J. Gibson and M. F. Ashby, *Cellular Solids: Structure and Properties*. Cambridge: Cambridge University Press, 2 ed., 1997.

[3] T. A. Schaedler and W. B. Carter, "Architected Cellular Materials," 7 2016.

[4] A. A. Zadpoor, "Mechanical meta-materials," 9 2016.

[5] P. M. Reis, H. M. Jaeger, and M. van Hecke, "Designer Matter: A perspective," *Extreme Mechanics Letters*, vol. 5, pp. 25–29, 12 2015.

[6] J. B. Pendry, "Negative Refraction Makes a Perfect Lens," tech. rep., 2000.

[7] Ergin T., Stenger N., Brenner P., Pendry J. B., and Wegener M., "Three-Dimensional Invisibility Cloakat Optical Wavelengths," *Science*, vol. 328, pp. 337–339, 6 2010.

[8] M. Kadic, T. Bückmann, R. Schittny, and M. Wegener, "Metamaterials beyond electromagnetism," 12 2013.

[9] M. Kadic, G. W. Milton, M. Van Hecke, and M. Wegener, "3D Metamaterials," tech. rep.

[10] K. Bertoldi, V. Vitelli, J. Christensen, and M. Van Hecke, "Flexible mechanical metamaterials," 10 2017.

[11] G. N. Greaves, A. L. Greer, R. S. Lakes, and T. Rouxel, "Poisson's ratio and modern materials," 2011.

[12] J. N. Grima, D. Attard, R. Caruana-Gauci, and R. Gatt, "Negative linear compressibility of hexagonal honeycombs and related systems," *Scripta Materialia*, vol. 65, pp. 565–568, 10 2011.

[13] J. N. Grima, R. Caruana-Gauci, D. Attard, and R. Gatt, "Three-dimensional cellular structures with negative Poisson's ratio and negative compressibility properties," *Proceedings of the Royal Society A: Mathematical, Physical and Engineering Sciences*, vol. 468, pp. 3121–3138, 10 2012.

[14] Y. C. Wang and R. S. Lakes, "Extreme stiffness systems due to negative stiffness elements," *American Journal of Physics*, vol. 72, pp. 40–50, 1 2004.

[15] H. Xu and D. Pasini, "Structurally efficient three-dimensional metamaterials with controllable thermal expansion," *Scientific Reports*, vol. 6, 10 2016.

[16] J. Li, Q. Yang, N. Huang, and R. Tao, "A novel mechanical metamaterial with tailorable Poisson's ratio and thermal expansion based on a chiral torsion unit," *Smart Materials and Structures*, vol. 30, 11 2021.

[17] M. Kadic, T. Bückmann, N. Stenger, M. Thiel, and M. Wegener, "On the practicability of pentamode mechanical metamaterials," *Applied Physics Letters*, vol. 100, 5 2012.

[18] T. Bückmann, M. Thiel, M. Kadic, R. Schittny, and M. Wegener, "An elasto-mechanical unfeelability cloak made of pentamode metamaterials," *Nature Communications*, vol. 5, 6 2014.

[19] T. Bückmann, R. Schittny, M. Thiel, M. Kadic, G. W. Milton, and M. Wegener, "On three-dimensional dilational elastic metamaterials," *New Journal of Physics*, vol. 16, 2014.

[20] L. R. Meza, S. Das, and J. R. Greer, "Strong, lightweight, and recoverable three-dimensional ceramic nanolattices," tech. rep.

[21] Zheng X., Lee H., Weisgraber T. H, Shuster M., DeOtte J., Duoss E. R., Kuntz J. D., Biener M. M., Ge Q., Jackson J. A., Kucheyev S. O., Fang N. X., and Spadaeeinil C. M., "Ultralight, ultrastiff mechanical metamaterials," *Science*, vol. 344, no. 6190, pp. 1373–1377, 2014.

[22] B. Walker and https://citationgecko.azurewebsites.net/, "Citation Gecko," 4 2020.

[23] T. Chen, M. Pauly, and P. M. Reis, "A reprogrammable mechanical metamaterial with stable memory," *Nature*, vol. 589, pp. 386–390, 1 2021.

[24] X. Ma and P. Yan, "Reprogrammable Mechanical Metamaterials with Heterogeneous Assembly of Soft Shell-Based Voxels," *Advanced Engineering Materials*, p. 2201323, 10 2022.

[25] X. Xia, C. M. Spadaccini, and J. R. Greer, "Responsive materials architected in space and time," 9 2022.

[26] D. Restrepo, N. D. Mankame, and P. D. Zavattieri, "Phase transforming cellular materials," *Extreme Mechanics Letters*, vol. 4, pp. 52–60, 9 2015.

[27] J. Shi, H. Mofatteh, A. Mirabolghasemi, G. Desharnais, and A. Akbarzadeh, "Programmable Multistable Perforated Shellular," *Advanced Materials*, vol. 33, 10 2021.

[28] B. Florijn, C. Coulais, and M. Van Hecke, "Programmable mechanical metamaterials," *Physical Review Letters*, vol. 113, 10 2014.

[29] J. Ding and M. Van Hecke, "Sequential snapping and pathways in a mechanical metamaterial," *Journal of Chemical Physics*, vol. 156, 5 2022.

[30] L. J. Kwakernaak and M. van Hecke, "Counting and Sequential Information Processing in Mechanical Metamaterials," 2 2023.

[31] H. Yasuda, P. R. Buskohl, A. Gillman, T. D. Murphey, S. Stepney, R. A. Vaia, and J. R. Raney, "Mechanical computing," 10 2021.

[32] A. Ion, L. Wall, R. Kovacs, and P. Baudisch, "Digital mechanical metamaterials," in *Conference on Human Factors in Computing Systems - Proceedings*, vol. 2017-May, pp. 977–988, Association for Computing Machinery, 5 2017.

[33] J. R. Raney, N. Nadkarni, C. Daraio, D. M. Kochmann, J. A. Lewis, and K. Bertoldi, "Stable propagation of mechanical signals in soft media using stored elastic energy," *Proceedings of the National Academy of Sciences of the United States of America*, vol. 113, pp. 9722–9727, 8 2016.

[34] Jin L., Khajehtourian R., Mueller J., Rafsanjani A., Tournat V., Bertoldi K., and Kochmann D. M., "Guided transition waves in multistablemechanical metamaterials," vol. 117, no. 5, pp. 2319–2325, 2020.

[35] J. A. Faber, J. P. Udani, K. S. Riley, A. R. Studart, and A. F. Arrieta, "Dome-Patterned Metamaterial Sheets," *Advanced Science*, vol. 7, 11 2020.

[36] J. P. Udani and A. F. Arrieta, "Taming geometric frustration by leveraging structural elasticity," *Materials and Design*, vol. 221, 9 2022.

[37] Singh A., Teunisse M., Labousse M., and van Hecke M., "Emergent computing in a non-Abelian metamaterial," 8 2023.

[38] C. Coulais, E. Teomy, K. De Reus, Y. Shokef, and M. Van Hecke, "Combinatorial design of textured mechanical metamaterials," *Nature*, vol. 535, pp. 529–532, 7 2016.

[39] T. Mei, Z. Meng, K. Zhao, and C. Q. Chen, "A mechanical metamaterial with reprogrammable logical functions," *Nature Communications*, vol. 12, 12 2021.

[40] S. Janbaz, K. Narooei, T. Van Manen, and A. A. Zadpoor, "Strain rate-dependent mechanical metamaterials," tech. rep., 2020.

[41] T. C. Lim, "A class of shape-shifting composite metamaterial honeycomb structures with thermally-adaptive Poisson's ratio signs," *Composite Structures*, vol. 226, 10 2019.

[42] W. Lv, L. Dong, and D. Li, "A novel metamaterial with individually adjustable and sign-switchable Poisson's ratio," *European Journal of Mechanics, A/Solids*, vol. 97, 1 2023.

[43] A. Farzaneh, N. Pawar, C. M. Portela, and J. B. Hopkins, "Sequential metamaterials with alternating Poisson's ratios," *Nature Communications*, vol. 13, 12 2022.

[44] M. F. Berwind, A. Kamas, and C. Eberl, "A Hierarchical Programmable Mechanical Metamaterial Unit Cell Showing Metastable Shape Memory," *Advanced Engineering Materials*, vol. 20, 11 2018.

[45] Z. Zhai, L. Wu, and H. Jiang, "Mechanical metamaterials based on origami and kirigami," 12 2021.

[46] J. L. Silverberg, A. A. Evans, L. Mcleod, R. C. Hayward, T. Hull, C. D. Santangelo, and I. Cohen, "Using origami design principles to fold reprogrammable mechanical metamaterials," tech. rep.

[47] H. Yasuda, T. Tachi, M. Lee, and J. Yang, "Origami-based tunable truss structures for non-volatile mechanical memory operation," *Nature Communications*, vol. 8, 12 2017.

[48] Z. Zhai, Y. Wang, and H. Jiang, "Origami-inspired, on-demand deployable and collapsible mechanical metamaterials with tunable stiffness," *Proceedings of the National Academy of Sciences of the United States of America*, vol. 115, pp. 2032–2037, 2 2018.

[49] N. Yang, C. W. Chen, J. Yang, and J. L. Silverberg, "Emergent reconfigurable mechanical metamaterial tessellations with an exponentially large number of discrete configurations," *Materials and Design*, vol. 196, 11 2020.

[50] J. T. Overvelde, T. A. De Jong, Y. Shevchenko, S. A. Becerra, G. M. Whitesides, J. C. Weaver, C. Hoberman, and K. Bertoldi, "A three-dimensional actuated origami-inspired transformable metamaterial with multiple degrees of freedom," *Nature Communications*, vol. 7, 3 2016.

[51] A. Iniguez-Rabago, Y. Li, and J. T. Overvelde, "Exploring multistability in prismatic metamaterials through local actuation," *Nature Communications*, vol. 10, 12 2019.

[52] W. Liu, H. Jiang, and Y. Chen, "3D Programmable Metamaterials Based on Reconfigurable Mechanism Modules," *Advanced Functional Materials*, vol. 32, 2 2022.

[53] A. Walther, "Viewpoint: From Responsive to Adaptive and Interactive Materials and Materials Systems: A Roadmap," 5 2020.

[54] C. Kaspar, B. J. Ravoo, W. G. van der Wiel, S. V. Wegner, and W. H. Pernice, "The rise of intelligent matter," 6 2021.

[55] Y. Gao, T. Ema, Z. Cao, S. Ni, E. Y. Chan, O. Tabata, T. Tsuchiya, X. Wang, and M. Wong, "A Planar Single-Actuator Bi-Stable Switch Based on Latch-Lock Mechanism," *2019 20th International Conference on Solid-State Sensors, Actuators and Microsystems and Eurosensors XXXIII, TRANSDUCERS 2019 and EUROSENSORS XXXIII*, pp. 705–708, 6 2019.

[56] Z. Sun, W. Bian, and J. Zhao, "A zero static power consumption bistable RF MEMS switch based on inertial generated timing sequence method," *Microsystem Technologies*, vol. 28, pp. 973–984, 4 2022.

[57] Z. Tang, Q. Tao, Z. Lan, Z. Liu, T. Tsuchiya, X. Wang, and M. Wong, "High Durability Latch-Lock Bi-Stable Switch on Y-Shaped Cantilever," in *21st International Conference on Solid-State Sensors, Actuators and Microsystems, TRANSDUCERS 2021*, pp. 675–678, Institute of Electrical and Electronics Engineers Inc., 6 2021.

[58] S. W. Huang, F. C. Lin, and Y. J. Yang, "A novel single-actuator bistable microdevice with a moment-driven mechanism," *Sensors and Actuators, A: Physical*, vol. 310, 8 2020.

[59] H. W. Huang and Y. J. Yang, "A MEMS bistable device with push-on-push-off capability," *Journal of Microelectromechanical Systems*, vol. 22, no. 1, pp. 7–9, 2013.

[60] ten Wolde M. and Farhadi D., "A single input state switching building block harnessing internal instabilities," 6 2023.

[61] J. Liu, W. Chen, H. Hao, and Z. Wang, "In-plane crushing behaviors of hexagonal honeycombs with different Poisson's ratio induced by topological diversity," *Thin-Walled Structures*, vol. 159, 2 2021.

[62] "Technical datasheet Prusament PLA," 2022.

[63] J. Djokikj, O. Tuteski, E. Doncheva, and B. Hadjieva, "Experimental investigation on mechanical properties of FFF parts using different materials," in *Procedia Structural Integrity*, vol. 41, pp. 670–679, Elsevier B.V., 2022.

[64] "Formlabs Materials Library," 2022.

[65] L. O. Chua, "Memristor—The Missing Circuit Element," *IEEE Transactions on Circuit Theory*, vol. 18, no. 5, pp. 507–519, 1971.

[66] C. Liu, L. Chen, H. P. Lee, Y. Yang, and X. Zhang, "A review of the inerter and inerter-based vibration isolation: Theory, devices, and applications," 9 2022.

[67] D. Biolek and Z. Biolek, "Predictive Models of Nanodevices," *IEEE Transactions on Nanotechnology*, vol. 17, pp. 906–913, 9 2018.

[68] D. Jeltsema and A. Dòria-Cerezo, "Mechanical memory elements: Modeling of systems with position-dependent mass revisited," in *Proceedings of the IEEE Conference on Decision and Control*, pp. 3511–3516, Institute of Electrical and Electronics Engineers Inc., 2010.

[69] Y. V. Pershin, S. La Fontaine, and M. Di Ventra, "Memristive model of amoeba learning," *Physical Review E - Statistical, Nonlinear, and Soft Matter Physics*, vol. 80, 8 2009.

[70] R. H. Lee, E. A. B. Mulder, and J. B. Hopkins, "Mechanical neural networks: Architected materials that learn behaviors," tech. rep., 2022.

[71] J. B. Hopkins, R. H. Lee, and P. Sainaghi, "Using binary-stiffness beams within mechanical neural-network metamaterials to learn IOP Publishing Smart Materials and Structures Smart Materials and Structures XX (2022) XXXXXX https://doi.org/XXXX/XXXX xxxx-xxxx/xx/xxxxxx 1 Using Binary-stiffness Beams within Mechanical Neural-network Metamaterials to Learn," 2023.

[72] R. Pfeifer and G. Gomez, "Morphological computation - Connecting brain, body, and environment," in *Lecture Notes in Computer Science (including subseries Lecture Notes in Artificial Intelligence and Lecture Notes in Bioinformatics)*, vol. 5436, pp. 66–83, 2009.

[73] K. S. Riley, S. Koner, J. C. Osorio, Y. Yu, H. Morgan, J. P. Udani, S. A. Sarles, and A. F. Arrieta, "Neuromorphic Metamaterials for Mechanosensing and Perceptual Associative Learning," *Advanced Intelligent Systems*, vol. 4, p. 2200158, 12 2022.

[74] M. A. McEvoy and N. Correll, "Materials that couple sensing, actuation, computation, and communication," 3 2015.

APPENDIX A

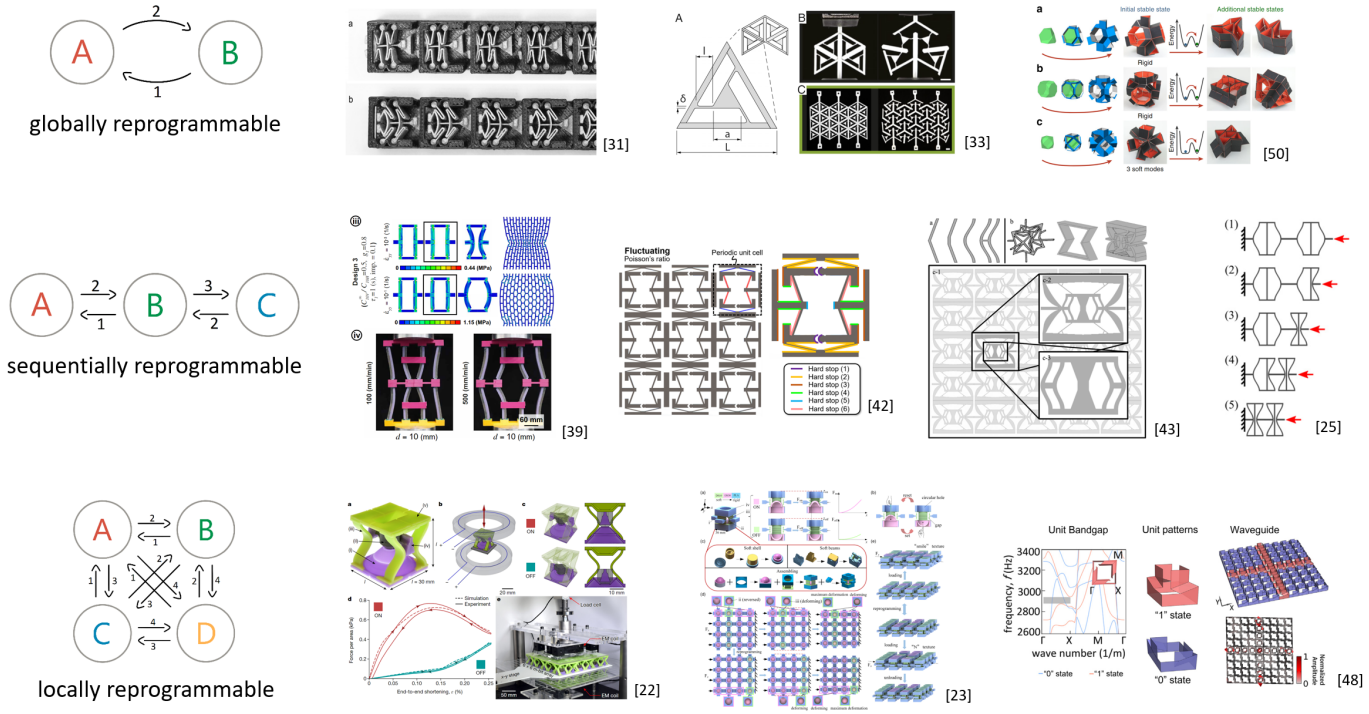

Fig. 12. Literature classification based on their state transition strategies.

APPENDIX B

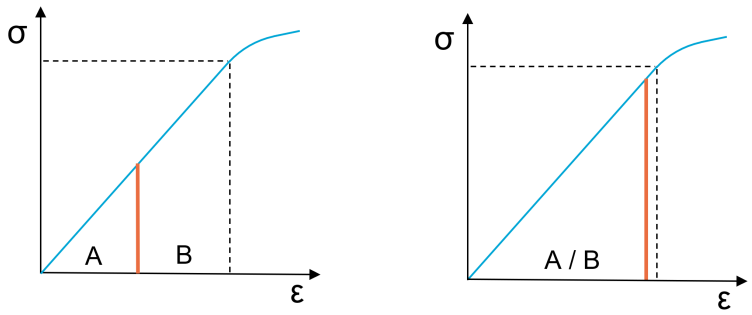

Fig. 13. Deformations in compliant mechanisms are stress-limited. The left stress-strain plot shows how bjection of input (displacement) and state (A or B) limits the displacement range per state. In the right stress-strain plot input and state are not linked, therefore both states can exercise the whole displacement regime until a set threshold is reached that causes the state transition (red line).

APPENDIX C

This paragraph provides additional information on potential future applications and interesting research trends, where adaptive property change of metamaterials, as proposed in this project, could potentially contribute. The ability of a mechanical metamaterial to change its property based on an input and its current state, combined with memory through non-volatility, indicates a potential for the application in mechanical memory devices, a mechanical analogy to Leon Chuas memristor concept [65]. Essentially creating mechanical metamaterials that could act as a mem-spring, mem-dashpot, mem-inerter [66], [67], [68]. Similar to how the memristor can be used to describe the learning behaviour of amoeba [69], mechanical memory devices could potentially be used to create mechanical neural networks that can learn behaviours and properties [70], [71]. Furthermore, integrated into a network of dynamically communicating unit cells, the proposed idea of state-dependent switching could potentially be used for morphological computing, where the morphology of the metamaterial is exploited in order to perform a kind of task distribution between controller, material, and environment [72], [73], [74].

APPENDIX D

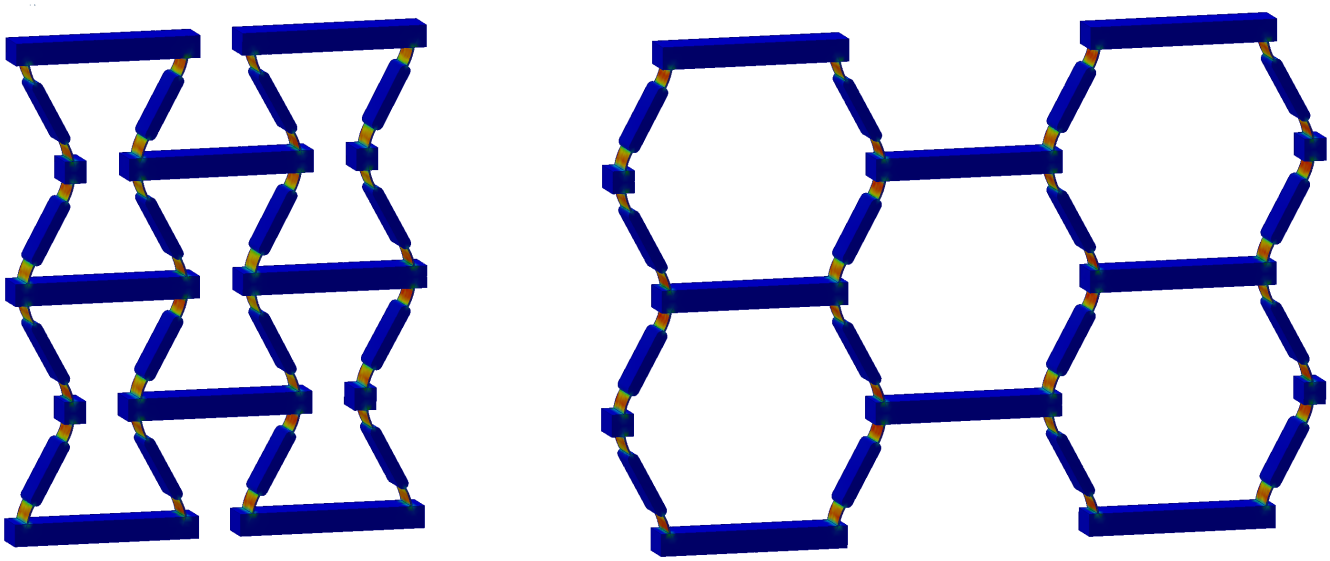

Fig. 14. Initial FEM analysis to validate the displacement behaviour of the hexagon tessellation. Both scenarios, negative Poisson's ratio (left) and positive Poisson's ratio (right), show the desired behaviour that stresses and strains are homogeneous across all unit cells. This is necessary to ensure that the states of all cells are accessible.

APPENDIX E

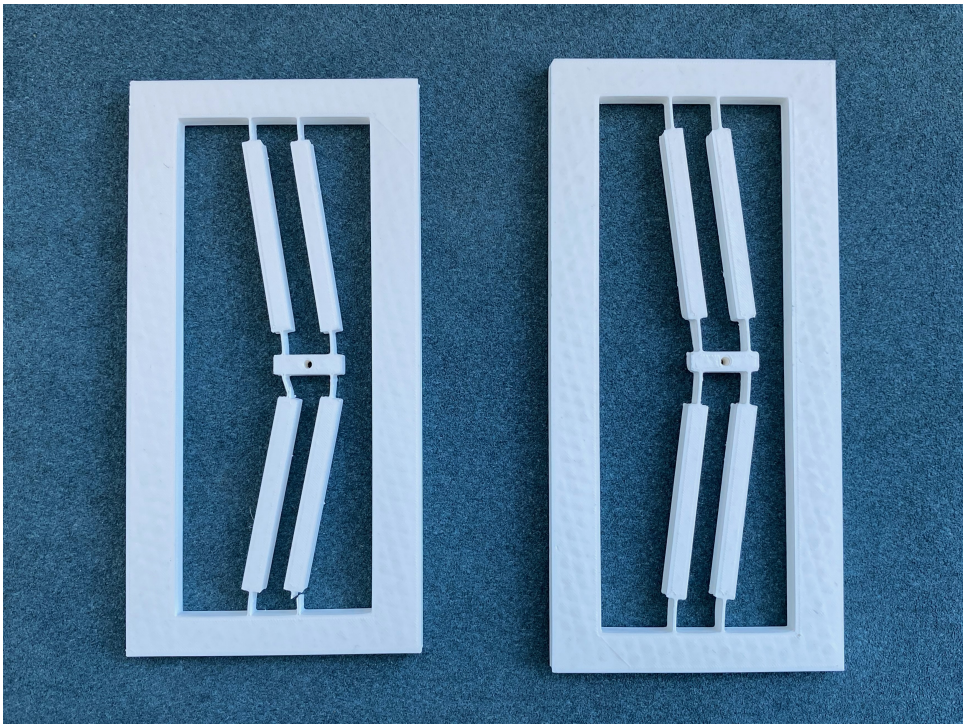

Fig. 15. PLA test prints of a simple bistable switch. The left print shows a fractured hinge due to the brittle characteristic of PLA.

APPENDIX F

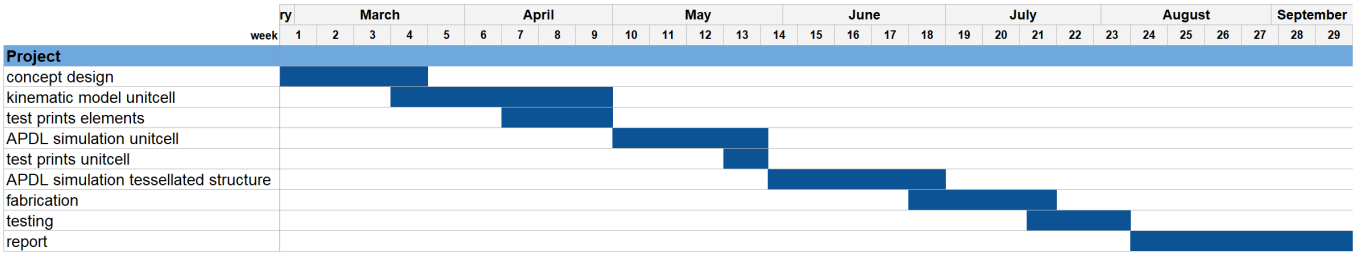

Fig. 16. Rough time schedule of the proposed thesis project.

Chapter 2

Technical Paper: Unit Cell with Sign-switching Poisson's Ratio for Adaptive Mechanical Metamaterials

Unit Cell with Sign-switching Poisson's Ratio for Adaptive Mechanical Metamaterials

— Technical Paper —

Luca Lagemann
Delft University of Technology
MSc Mechanical Engineering, High-Tech Engineering, Mechatronic System Design
Delft, Netherlands
l.lagemann@student.tudelft.nl

***Abstract*—Mechanical metamaterials are architected materials with unique properties derived from their internal structure, rather than the material they consist of. Introducing distinct stable states into the material architecture allows the creation of mechanical metamaterials with multiple effective properties that can be altered post-fabrication. So far these so-called reprogrammable mechanical metamaterials have only demonstrated responsive behaviour, where the state of the metamaterial is dictated by the external input, leading to complex actuation and limited functionality. This research introduces a transformative approach to overcome these limitations through state-dependent switching, enabling metamaterials to autonomously determine their state based on internal information. Leveraging internal instabilities in the form of bistable and slender buckling elements, a contactless and tessellatable 3D unit cell design that can switch between positive and negative Poisson's ratios upon a specified displacement threshold is introduced. State transition occurs based on internal state information, rather than the external input, enabling adaptive behaviour. Both, Finite Element Analysis (FEA) simulations and experimental validation demonstrate the ability of the unit cell to switch between positive and negative Poisson's ratio under the same repeated input. Preliminary FEA simulations further suggest that through the tessellation of this innovative unit cell, the adaptive behaviour can be exploited to create mechanical metamaterials capable of adaptive shape morphing and repeatable counting abilities.**

***Index Terms*—Adaptive, Mechanical Metamaterial, Poisson's Ratio, State-dependent Switching, Unit Cell**

I. Introduction

Mechanical metamaterials offer unique properties driven not by their composition but by their rationally designed structure. Particularly, their behaviour emerges from unit cells, which, when tessellated, create effective properties that can transcend those of its ingredient materials [1]. While the potential of mechanical metamaterials has been explored extensively [2] [3], their static nature post-fabrication remains a significant constraint.

The emerging sub-field of reprogrammable mechanical metamaterials seeks to address this by embedding multiple stable states within the material's architecture. By controlling and reconfiguring these states the effective material property can be altered as desired, even after fabrication. A comprehensive literature review was conducted on the current advancements in reprogrammable mechanical metamaterials. Various types of structures, like origami, kirigami, soft materials, combined with snapping instabilities or frustration have been explored [4] for a wide range of applications, such as reprogrammable stiffness [5], acoustics [6], Poisson's ratio [7] [8], energy absorption [9], shape morphing [10], signal transition [11] [12], and logic functions [13] [14]. A trend in the direction of high reconfigurability is noticeable, where the number of possible configurations is increased through the state change of individual unit cells [5] [6] [15], which requires complex actuation to reprogram the metamaterial structures. The work of [16] demonstrates that through strain mismatch, different material states can be accessed under the same input depending on the input speed. In another example, [7] contact points are used to achieve sequential deformations with alternating Poisson's ratios under the same input. However, these examples lack memory to be able to retain their state, require multiple materials, or rely on contact, which leads to microstiction, wear, and scalability issues. Furthermore, the state of the metamaterial is exclusively determined by the user's external input. This bijection between the state and the external input restricts the metamaterial functionality to responsive behaviour.

State-dependent switching is a promising alternative to the currently used input-dependent switching, which allows breaking the bijective link between external input and state by making use of internal state information. In recent work, a state-switching mechanism has been proposed that can switch between states under a single cyclic input through the use of quadratic stiffness elements [17]. Since it is contactless and scalable, this concept provides a useful strategy to integrate state-dependent switching into rational metamaterial design that allows switching between property states. This not only effectively reduces the number of actuators but also allows to advance from responsive to adaptive behaviour, paving the way for more intelligent mechanical metamaterials. Adaptive behaviour refers to the ability to adjust and respond to complex sensory environments. The concept necessitates understanding the role of memory and finding ways to modulate such memories by changing the energy landscape. For this objective, the material is required to be able to process internal information in the form of feedback. [18] [19]

This work presents a unit cell design with sign-switching Poisson's ratio states which can serve as a building block to create adaptive mechanical metamaterials. It integrates state-dependent switching through internal instabilities and associates Poisson's ratios of opposing signs to the two distinct states, to create a 3D tessellatable unit cell. Bistable elements are used to introduce memory to create a non-volatile state of the material property and guide the output deformation accordingly. The design is contactless, monolithic, and derives its property solely from its structural geometry. A simple displacement threshold is used to trigger state transition.

Section II of this report provides details on the unit cell design and its functionality, followed by numerical and experimental results, and potential metamaterial implementations. The results are discussed in Section III and opportunities for future work are highlighted in Section IV. Section V concludes the work of this project. Details on the materials and methods are provided in the Supplementary Material.

II. Results

Sign-switching Poisson's Ratio Unit Cell

In order to achieve Poisson's ratios of opposing signs, the design of the unit cell frame is inspired by the topology and deformation behaviour of hexagons. Figure 1 shows the 3D unit cell in A and its cross section in the two stable states in B. The first state resembles a hexagon with outward-pointing sides (green), whereas in state two the outline of the frame traces a re-entrant hexagon with inward-pointing sides (red). Under an axial compressive input displacement (blue arrows) the unit cell generates a lateral output motion, which determines the lateral strain. In its first state, the output motion is directed outward, leading to a positive Poisson's ratio, while in its second state the frame sides bend inwards, resulting in auxetic behaviour with a negative Poisson's ratio.

Alongside the frame, which dictates the deformation behaviour and therefore the effective Poisson's ratio, the unit cell consists of internal components that determine the current state and control its transition. The inner architecture of the cell can be reduced to three main components, which are highlighted in Figure 2. The bistability of the yellow state element is used to define the current state of the material property (Poisson's ratio) in a non-volatile fashion, which adds a form of memory to the unit cell. The second bistable element, marked in purple, is designed to have a certain non-linear force-displacement profile that allows it to generate a tensile force in the positive y-direction as well as a tensile followed by compression force in the negative y-direction. This allows the non-linear spring to position the frame's side beams depending on the position of the state element, essentially "reading" the unit cell memory and guiding the output accordingly. The frame, state element, and non-linear spring are connected via a central transmission mechanism (blue), that transmits forces and displacement between the components.

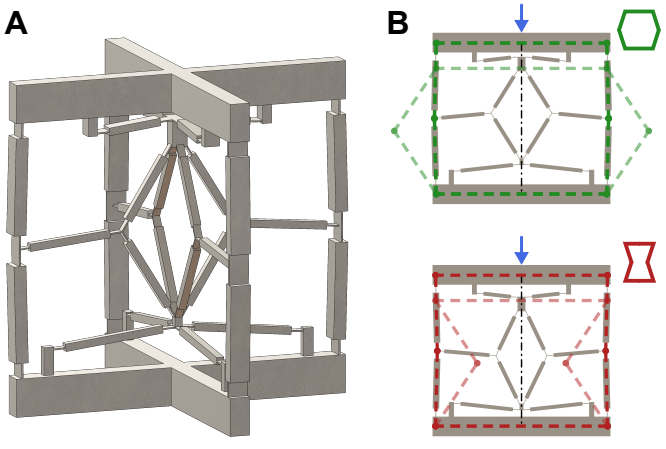

Fig. 1. Proposed 3D unit cell design and its two stable states. **A** Isometric view of the 3D unit cell design. **B** Cross section of the unit cell in the hexagon state with positive Poisson's ratio, where an axial compression indicated by the blue arrows causes lateral expansion (top). In the re-entrant state (bottom) the same input leads to the opposite output motion and therefore a negative Poisson's ratio.

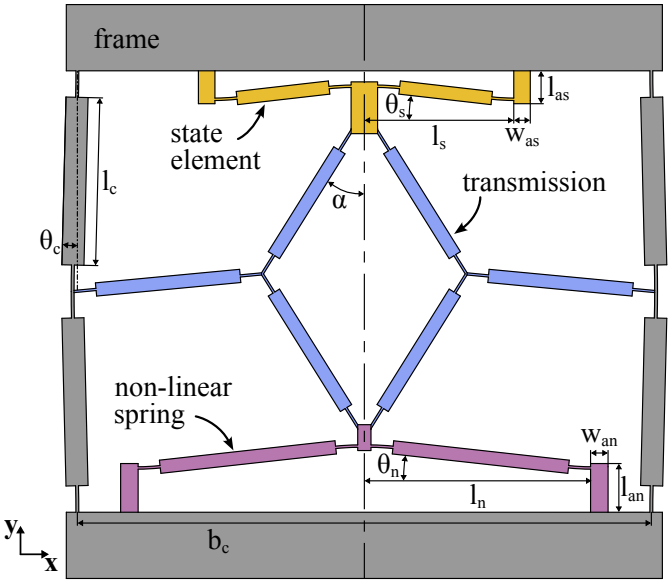

Fig. 2. Components of the unit cell design and important design parameter.

When an axial compression is applied to the unit cell in the initial configuration, the outward motion of the frame sides stretches the transmission mechanism, resulting in a vertical contraction of the rhombus shape. This generates a pulling force on its top and bottom endpoints which are connected to the state element and non-linear spring respectively. Once a certain threshold is reached, the state element snaps to its second stable position. At this point, the new state information is "written" to the unit cell memory. While releasing the compressive input, the vertical displacement of the state element and the inward motion of the frame sides shift the transmission mechanism downwards, causing the non-linear spring to switch to its second position if certain criteria are met. In this position, the combined displacement of the state element, the non-linear spring, and the transmission mechanism have shifted the frame sides inwards by a displacement d_x, crossing their bifurcation point, as visualized in Figure 3A. This configuration represents the re-entrant unit cell shape. With the following loading cycle, the frame sides

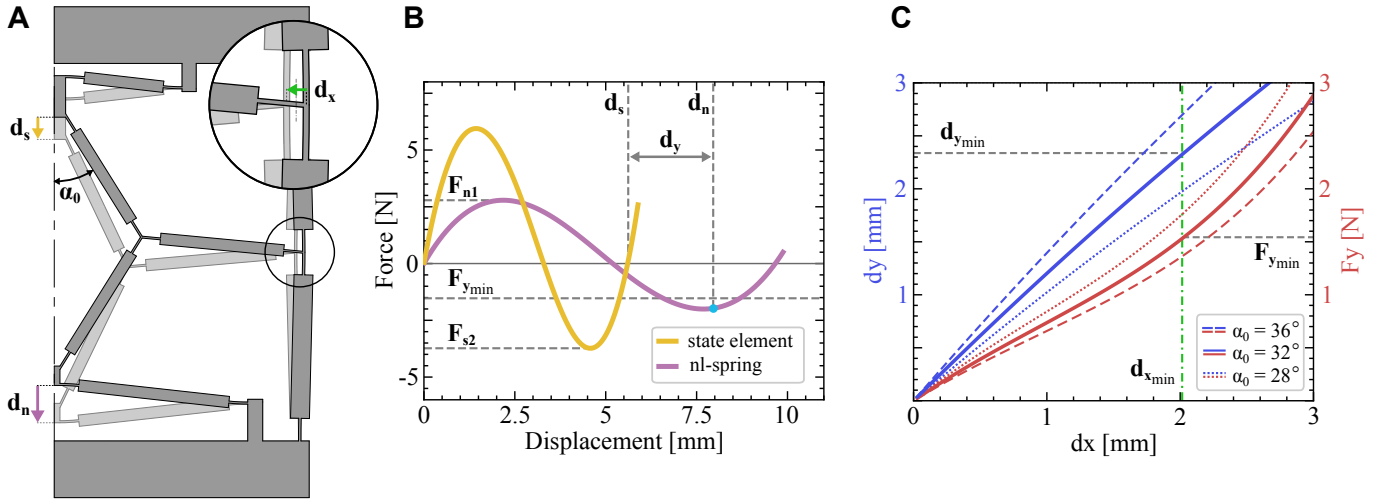

Fig. 3. Internal displacements and forces of the unit cell. **A** Right half of the unit cell shown in its two stable states, highlighting the displacements of the states element d_s, the non-linear spring d_n and the frame sides d_x. **B** Force-displacement characteristics of the state element and the nonlinear spring including important limits derived from functional requirements, e.g. minimum lateral displacement d_x. **C** Required vertical force F_y and displacement d_y, by which the central rhombus needs to be stretched vertically to generate a desired lateral displacement of the frame sides d_x.

bend inwards, representing its negative Poisson's ratio state. Now the inward motion compresses the rhombus laterally, which generates a pushing force on the state element and the non-linear spring. Again, once a threshold is reached, the state element snaps back and the original state is "written" to its memory. While the compressive input is being removed, the transmission mechanism and the non-linear spring return to their initial position, switching the unit cell back to its hexagonal shape with a positive Poisson's ratio.

To accomplish this deformation behaviour, the non-linear spring and state element must fulfil certain force-displacement criteria, as demonstrated in [17]. The force-displacement plots of the state element and non-linear spring, shown in Figure 3B provide insights to validate these criteria. Firstly, the second critical force of the state element F_{s2} needs to be sufficiently larger than the first critical force of the non-linear spring F_{n1}. This is required to ensure that, after state transition, the non-linear spring switches before the state element snaps back. Furthermore, the force of the nonlinear spring F_n at a displacement of $d_n = d_y + d_s$ (highlighted by the light blue marker) is required to be larger or equal to F_y. Ideally, at this point F_n is closest to its minimum, such that as much force as possible is generated. F_y is the force and d_y is the displacement by which the rhombus needs to be stretched vertically in order to displace the frame sides by d_x to the re-entrant position.

The rhombus shape of the transmission mechanism introduces a geometric advantage that can be exploited to amplify forces or displacements in the system by the definition of its initial angle α_0. Figure 3C plots the vertical stretch of the rhombus (d_y) and corresponding force (F_y) over the lateral displacement of the frame sides (d_x) for a range of α_0. Due to the lever effect, larger values of α_0 result in larger F_y and lower d_y, while smaller α_0 angles have the opposite effect. For the design of the bistable elements, it is desired to have a low F_y as well as d_y. An α_0 angle of 32 degrees turned out to be a good trade-off. Further analysis on the effect of α_0 on the overall unit cell behaviour can be found in the Supplementary Material Section V.

For chosen frame dimensions of l_c = 38mm, b_c = 130mm, t_c = 8mm, θ_c = 1.4deg and frame flexures of 6mm length and 0.65mm width, the initial position of the midpoint of the frame side beams is 1.0075mm from the central bifurcation point. Therefore d_x was chosen to be at least 2.015mm to achieve a robust re-entrant state. With a defined value for a desired d_x the minimum vertical force F_{ymin} and displacement d_{ymin} can be derived, as shown in Figure 3C. These values are used as limits for the force-displacement graphs of the non-linear spring and state element, as stated in the criteria above. Through parametric studies, a large amount of state element and non-linear spring designs were generated, which were then filtered by stress limitation and these criteria. Further information on the selection process can be found in the Supplementary Material Section I-D.

Table I shows the selected design parameters, which were used in the FEA model of the unit cell and for fabrication. It is important to note that the parametric sweep was conducted to reduce the large design space and identify potential parameter combinations. Therefore, the chosen dimensions don't represent an optimal solution but rather a functional combination according to the defined criteria.

TABLE I
DESIGN PARAMETERS FOR THE STATE ELEMENT AND NON-LINEAR SPRING.

	design parameters						
	θ [deg]	l [mm]	w_a [mm]	l_a [mm]	l_f [mm]	w_f [mm]	t [mm]
state element	6.5	26	3.75	6.45	5	0.55	6
non-linear spring	6.3	45	4	10	5	0.55	3

Numerical and Experimental Results

The functionality and performance of the proposed unit cell design were analysed and validated using FEA and experimental measurement of a 3D printed prototype. The FEA was set up as a non-linear (large displacements) static analysis with a linear elastic material model and the geometry was modelled using two-node beam elements. A cyclic displacement of 1.5mm in negative y-direction was applied to the top central node, while the bottom central node was fixed in all degrees of freedom. The prototype was 3D printed using stereolithography (SLA) with the material tough2000, which has a Young's Modulus of 2.2GPa. A tensile test machine was used to apply the same input displacement as in the FEA, at a fixed rate of 10mm/min and one minute pause between each loading cycle. Further details on the FEA procedure, the fabrication process, and the experimental measurement can be found in the Supplementary Materials.

Figure 4 summarizes the results of both FEA and experimental measurement. Snapshots of representative stages during two consecutive loading cycles from FEA and experiment are shown in 4A and 4B respectively. Both confirm the desired geometrical changes and deformation. At stage I, the unit cell is in its initial hexagonal configuration. Under compression, it expands laterally. The colour contour shows the displacement

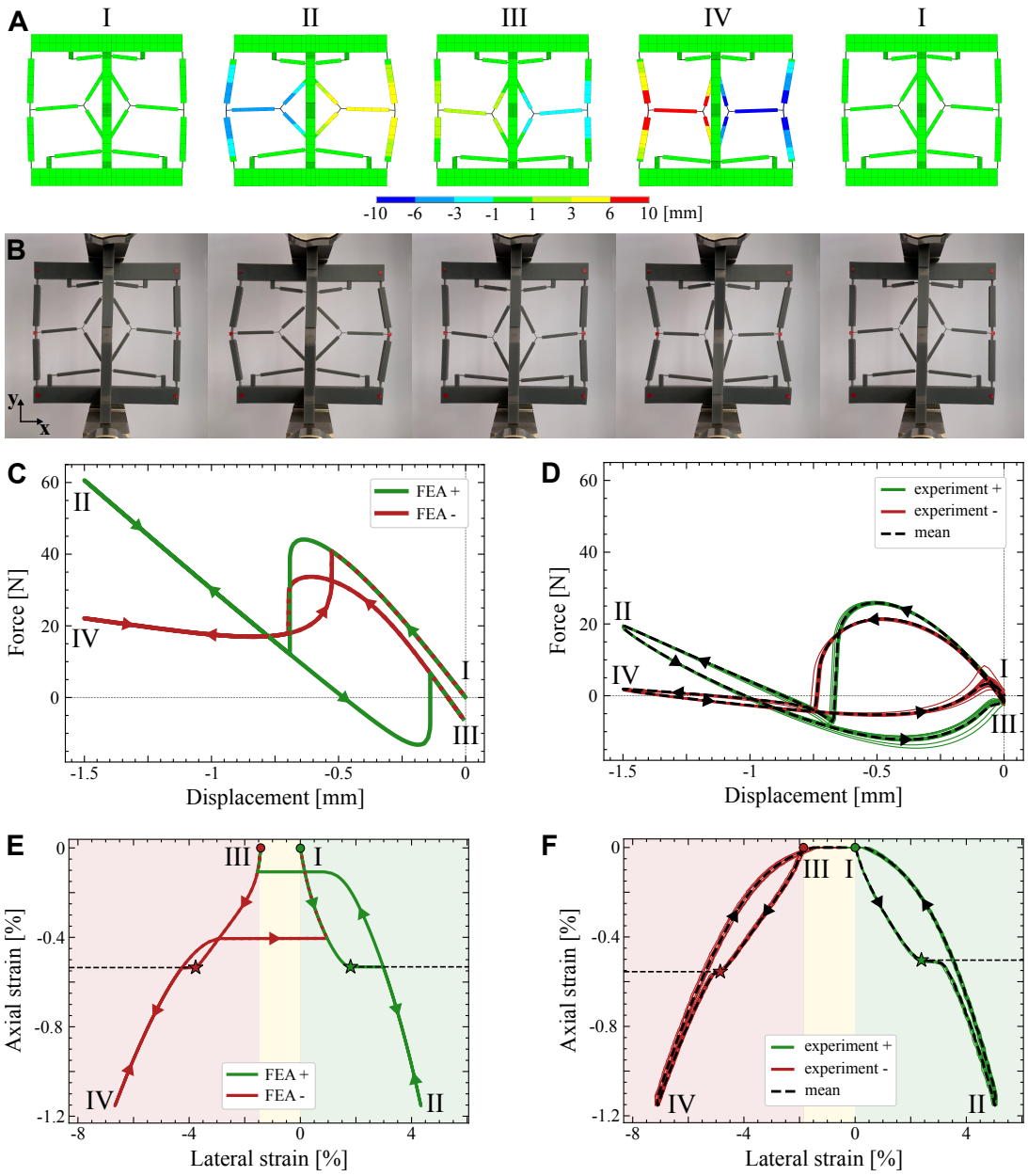

Fig. 4. Numerical and experimental results of the developed unit cell. **A** FEA deformation sequence of the unit cell under two consecutive loading cycles with an axial compression of 1.5mm as the input. The colour map graphs the lateral displacement. **B** Deformation sequence captured from the experimental measurement, showing the unit cell at the equivalent loading stages. Red markers were used for capturing the lateral displacement. **C** and **D** show the force-displacement results from FEA and experiment respectively. The green graph shows the force profile between stage I and stage III (positive Poisson's ratio state), while red represents stages III to IV and back to I (negative Poisson's ratio state). Arrows on the graph indicate the displacement direction. **E** and **F** graph the results of the deformations from FEA and experiment, showing the input-output relation and Poisson's ratio as well as state transition behaviour.

in x-direction, indicating a positive Poisson's ratio. At full input displacement (stage II) the state element has switched to its second stable position. Once the input displacement is removed (stage III), the non-linear spring has switched as well and the frame sides are shifted inwards. At this point, the unit cell is in its re-entrant configuration, where the input displacement causes lateral contraction, as shown in stage IV. Finally, when the input displacement is removed, the unit cell returns to its initial configuration from stage I.

To analyse the switching behaviour, the force profile is plotted over the input displacement for both loading cycles. Figure 4C and 4D show the force-displacement profile from FEA and experiment respectively. The four stages described above are labelled in the plot and the force profile of the positive Poisson's ratio state is shown in green and the negative Poisson's ratio state in red. The peaks represent the required switching force, which occurs during loading, when the state element switches, between stages I and II and between III and IV. FEA results predict these forces to be 44.1N and 33.7N, whereas the experimental results show 25.9N and 21.4N respectively. A sudden force drop indicates the switching event of the state element, whereas a sudden increase in force occurs when the non-linear spring switches and the frame sides pass the bifurcation point. In the FEA, the state element switches at an input displacement of -0.7mm for both positive and negative Poisson's ratio state. In the experiment, an input displacement of around -0.65mm led to switching for the positive and -0.72mm for the negative Poisson's ratio states. In both FEA and experiment, the graphs show an almost constant force after the switching event in the negative Poisson's ratio state, indicating a very low stiffness of the unit cell in the configuration shown in stage IV.

The Poisson's ratio of both unit cell states can be analysed by looking at the axial and lateral strain, as shown in Fig. 4E and 4F. The input displacement divided by the initial height of the unit cell represents the axial strain. The lateral strain is the added horizontal displacement of the frame side centre points divided by their initial distance. Red markers were placed on the prototype and tracked using image processing to capture the lateral displacement of the frame sides. The zone in between the initial positions, shaded in yellow, is the transition zone, where the frame switches between hexagonal and re-entrant configurations. Its width represents the displacement of the frame sides under state change (d_x). The experimental results show a larger d_x, which means that the frame sides have been displaced further, indicating larger margins to the bifurcation point. Furthermore, state transition in the experiment takes place when the axial strain is near zero, whereas in the FEA results, this happens significantly earlier. This is particularly noticeable in the negative to positive Poisson's ratio state transition, where switching occurs at -0.53mm. This is accompanied by a drastic increase in force that is visible in the force-displacement plot at this switching event.

The effective range, in which the unit cell can sustainably utilize its Poisson's ratio property lies between the initial position of both states, highlighted by the circular marker, and their respective switching point (star marker). The Poisson's ratio ν = - $\epsilon_{lateral}$ / ϵ_{axial} represents the inverse of the slope in the strain plots. For the derived numerical data, the Poisson's ratio is calculated using finite difference. The FEA results show a Poisson's ratio range from 2.54 to 14.13 and -1.53 to -12.75 for the two unit cell states. From the experimental data, these range from 5.16 to 14.3 and -5.62 to -13.41.

Metamaterial Implementations

By connecting multiple unit cells into a tessellated arrangement, a mechanical metamaterial can be designed that leverages the demonstrated unit cell behaviour. Figure 5 showcases the potential of the developed unit cell to serve as a building block for expansive metamaterial structures.

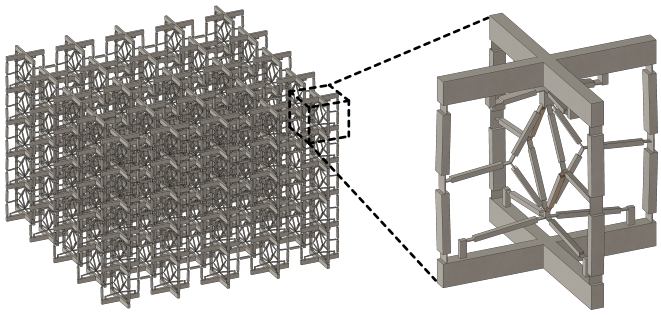

Fig. 5. Conceptual representation of a 3D mechanical metamaterial constructed with the developed unit cell building block.

To analyse how the demonstrated unit cell behaviour translates in a metamaterial, different tessellation strategies were investigated using FEA. In these studies, the width of the horizontal frame beams was increased from 15mm to 22mm, to avoid influences from switching neighbouring cells. A 2x2x2 tessellation, where four sets of two in series connected unit cells are placed in parallel, is shown in Figure 6A. A horizontal link is introduced to connect lateral neighbouring cells at their output (midpoint of frame sides). Figure 6B shows the deformation behaviour of the 2x2x2 metamaterial for four consecutive loading cycles. The two stable states of the metamaterial are indicated by the green and red dashed lines. In the first and third cycles, the axial input strain is kept below a certain level, such that no switching occurs and the metamaterial remains in its current Poisson's ratio state. Once an input is applied that is large enough to generate a lateral strain that passes the switching threshold (indicated by the horizontal grey dashed lines), the internal energy landscape of the metamaterial is modulated and state change occurs, as shown in loading cycles 2 and 4. The force needed to induce a state change has increased almost fourfold, and the displacement has nearly doubled in comparison to a single unit cell. This suggests that the 2x2x2 metamaterial exhibits twice the stiffness of the single unit cell, which is expected considering the series and parallel arrangement of the tessellation.

Stacking multiple unit cells on top of each other forms a series connection, where the stiffness characteristic of the unit cell states can be exploited to create a metamaterial that acts like a mechanical counter. The positive and negative Poisson's ratio states can be interpreted as binary values 1 and 0 respectively. An example based on three unit cells is shown in Figure 6C and D. For this example, a small defect

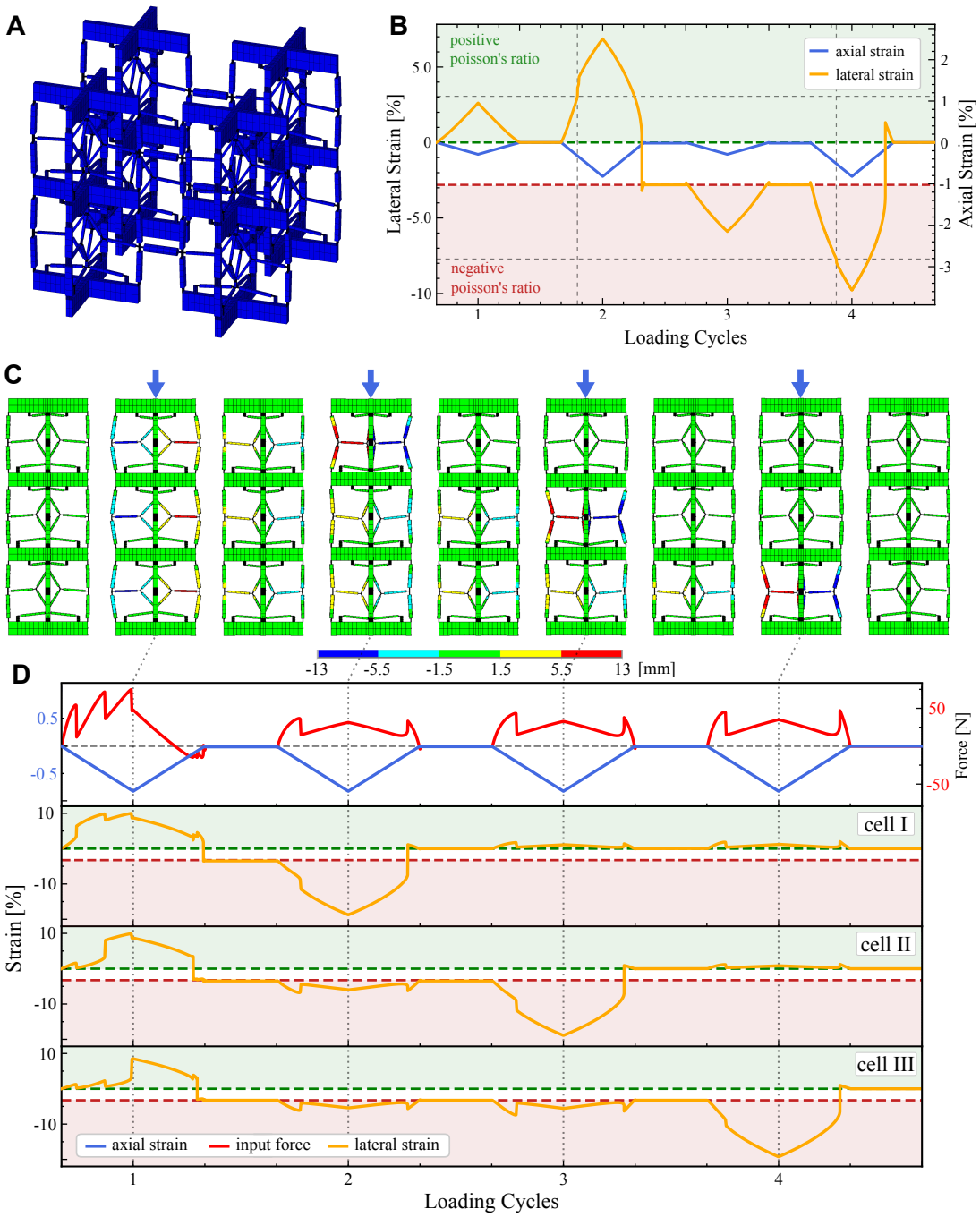

Fig. 6. Results of preliminary metamaterial implications of the unit cell. **A** FEA model of a 2x2x2 unit cell tessellation. **B** Displacement behaviour of the 2x2x2 metamaterial over four loading cycles demonstrating its adaptive behaviour capability by switching between positive and negative Poisson's ratio state under the same repeated input. **C** Deformation sequence of a 1x1x3 tessellation with counting ability. The colour map shows the lateral displacement. **D** FEA results from the deformations sequence shown in C, highlighting the deformation, current state and switching events of the three unit cells at each load step.

is introduced to guide the order in which the individual cells switch. The key to achieving this functionality is the distinct post-switching stiffness of the unit cell. While the stiffness of the unit in its 1-state (positive Poisson's ratio) remains high after the state element has switched, the 0-state (negative Poisson's ratio) has a low, near zero post-switch stiffness. This allows all three unit cells to switch from their 1- to 0-state within one loading cycle, as shown in the first loading cycle in Figure 6C and D. This load step also requires the highest input force (red curve). Once all cells are in their 0-state, the same input only causes one unit cell to switch, because the full input displacement is absorbed by the low stiffness of the cell that has switched first. In this case cell I, as can be seen by its large lateral strain in the negative Poisson's ratio regime (see the second cycle of Fig. 6D). With the following loading cycles, only individual 0-state cells switch, until the initial configuration with all three unit cells in their 1-state is restored and the cycle can start over.

III. Discussion

The switching behaviour of the developed unit cell design shows good agreement between FEA and experimental measurement results, which is the most significant trade to demonstrate the state-dependent switching capability. The results show that the unit cell in fact can switch between its two property states on the same repeated input by making use of internal information of its current state.

For the displacement thresholds, on which the cell switches its state, the experimental result only deviates less than 8% from the FEA result. However, the switching forces show a large discrepancy, with a factor of about 1.7. This deviation can be explained by the fact that the material of the prototype shows viscoelastic behaviour. The hysteresis in the plots of the experimental results indicates that energy is dissipated due to the damping capacity of the material. Viscoelastic behaviour in the form of stress relaxation was also identified in experiments on individual bistable elements, where the critical switching force varied depending on the rate at which the load was applied (see Supplementary Materials Section IV-B). Further discrepancies may be caused by manufacturing or post-processing procedures. Due to its thin flexures, the thickness variation throughout the unit cell structure is quite large, which can cause differences in material properties because some parts cure quicker than others. The most significant difference between FEA and experimental results is the state transition behaviour. In the experiment, the unit cell changes its state, when the input strain is almost back to zero, whereas the FEA shows a more direct switching behaviour associated with high forces. These deviations are again a consequence of the viscoelastic material property of the prototype.

The derived values for the effective Poisson's ratio that can be sustained in each state are quite high. This is expected, since the initial angle of the frame sides is very steep, leading to large lateral displacements under small axial input displacement. Due to the same reason, the axial range of motion of the unit cell is relatively low. The Poisson's ratios from the experiment show higher initial values than the FEA results, indicating more lateral displacement for the same axial input displacement. This can partly be attributed to the fact that d_x, the lateral displacement of the frame sides under state transition, is larger in the experimental results than in the FEA. A larger d_x causes a larger initial angle of the frame sides, allowing for quicker lateral displacements. In the FEA the frame sides are closer to vertical and seem to undergo axial compression before entering lateral displacement. The larger value of d_x in the experiment is likely to be caused by stress relaxation. As the FEA result shows, the second state of the unit cell exerts a small negative force at zero displacement. The time in between loading cycles during the experiment allowed the unit cell to compensate for the internal stresses introduced by holding it at zero displacement, by pulling the frame sides further inward.

It is important to note that the derived design parameters represent just one working design, compromised by the chosen manufacturing process and material of the prototype. Specifically, the overall size of the unit cell was confined by the maximum build volume of the 3D printer and at the same time long, thin features were prone to warp, which limited the flexure design. This has led to a rather stiff design, which shows aggressive state-changing behaviour in the FEA. In some cases, the simulation found another equilibrium solution, where during the transition from negative to positive Poisson's ratio state, the frame sides are pushed too far outward, causing unexpected snapping of the state element. This behaviour is not expected to happen in a physical system due to the energy dissipation. Increasing the width of the horizontal frame beam also helped to delay the state transition and mitigate this behaviour. Earlier designs where long-length flexures were used for the transmission mechanism were more robust due to their distributed compliance but turned out not to be manufacturable with the chosen fabrication process.

Different types of metamaterials can be developed by connecting multiple unit cells. Preliminary FEA has shown interesting emerging properties. The simulated deformation behaviour of a simple 2x2x2 tessellation shows the ability of the metamaterial to switch between two states (positive and negative Poisson's ratio) under a cyclic input based on the current state. A threshold is used to trigger modulation of the internal energy landscape and thereby change the material property. The ability to use internal state information to rewrite the 'memory' (property state) of the metamaterial demonstrates the potential of the developed unit cell to be used for adaptive property change. In this particular FEA study, state change occurs uniformly and globally. However, the adaptive behaviour could be extended to other circumstances, with different initial configurations or boundary conditions. Experimental simulations of a planar 2x1x3 tessellation show that the adaptive behaviour can be used as a learning ability for shape morphing (see Supplementary Material Section V-B). First, specific boundary conditions are applied under loading, which only causes some unit cells to change their state. With the following loading cycles below the switching threshold, the structure expresses the deformation behaviour it has learned from the previous input, even when the boundary conditions are removed. Subsequent loading cycles above the switching threshold could be used to reset the metamaterial and learn a new shape. This behaviour can be seen as a form of associative learning (Pavlovian adaption) [18].

Even though FEA simulations on tessellations larger than 2x2x2 were not completed successfully for two complete loading cycles, preliminary results showed that state change from negative to positive Poisson's ratio doesn't occur on the metamaterial level but rather at individual unit cell level. The reason is the unit cell's low post-switching stiffness at this stage. Multiple loading cycles would be needed to return the metamaterial structure to its initial state. A potential strategy to prevent this is to use a type of honeycomb tessellation (see Supplementary Material Section V-C). This arrangement is expected to promote simultaneous switching since unit cell frame sides are shared and rows of cells are not isolated. Therefore, if one cell switches, its neighbours should switch as well, causing a chain reaction throughout the metamaterial. This could potentially also be used for signal transmission, where the same input can be used for transmission and

resetting.

Unit cells connected in series show an evolutionary state change, which could be used as a mechanical counter that counts the number of loading cycles above a certain threshold. Additionally, when a unit cell changes its state, its height is increased for a short moment as the frame sides cross the bifurcation point. This axial extension in combination with certain thicknesses of the horizontal frame beam can cause interference between neighbouring unit cells, which has been witnessed to introduce unexpected switching. In the context of the mechanical counter, this could be used to achieve more complex counting algorithms, like binary or grey code. Furthermore, the states of the unit cell can be seen as a type of stable memory that stores information from the previous loading cycle.

However, stress limits were not considered in this tessellation and the simulations of larger structures often showed convergence problems due to rigid body motion on state transition. Further analysis needs to be done on the tessellation of the unit cell, to fully explore its potential.

IV. Future Work

This study has demonstrated and validated state-dependent switching between positive and negative Poisson's ratio on unit cell level. Further work needs to be done to translate the emerging adaptive behaviour to real metamaterial implementations. Tessellated structures, as shown in the preliminary FEA, should be extended and validated by fabrication and experimental measurement. The FEA should be improved to achieve better convergence since the simulations of larger structures often fail to converge due to warp limit violation, indicating rigid body motion. One could investigate different boundary conditions, for example, the implementation of 'weak springs'. For the fabrication of larger tessellations, it is recommended to use a process that is robust and suitable for miniaturization.

Analysing unit cell interactions and including information from neighbouring cells in the state control is another interesting direction that could enhance the capabilities and autonomy of such metamaterials. A potential method would be to investigate the width of the horizontal frame beam which has been shown to have an influence on the bistability and switching behaviour of neighbouring cells. Furthermore, different types of tessellation could be explored, such as a honeycomb tessellation.

Even though the next steps should focus on the tessellation of the unit cell to validate the adaptive behaviour on the metamaterial level, further individual improvements can be made to the unit cell design as well. For example, one could increase the displacement range by clever implementation of springs. Another interesting approach would be to use S-buckling with off-centre actuation for the state element to introduce different load paths for the forward and backward actuation [20]. The different load paths could be exploited to delay the state switching event and thereby gain more range of motion. Furthermore, since the current design is quite stiff, the performance and robustness of the unit cell could potentially be improved by moving from notched compliance to distributed compliance. One could also perform a parameter optimization, to exploit the full potential of the unit cell design for a certain use case or behaviour, like specific switching force or displacement. The developed unit cell can easily be tuned to achieve different switching thresholds. An interesting research direction would be to investigate its potential for other material properties. The results show that different stiffness states are achievable, therefore adaptive stiffness could be further investigated.

Future work could also involve extending the static model to a dynamic model, which can incorporate damping behaviour from the chosen base material and explore the dynamic performance of the unit cell and its tessellations. Although this work provides an APDL script that efficiently generates metamaterial tessellations of the designed unit cell, finding the right solver settings to achieve a converging solution was tedious and time-consuming. Therefore other approaches to model large metamaterial structures could be explored.

Furthermore, the identified viscoelastic behaviour causes an effect of the actuation speed on the internal forces of the unit cell. This time dependency could potentially be exploited as another input dimension, where the time the input is being applied influences the switching threshold.

V. Conclusion

A metamaterial unit cell design was introduced that can switch between positive and negative Poisson's ratio states under the same repeated input. Through internal instabilities in the form of bistable elements, it is able to change its state based on a displacement threshold and its current state, rather than solely dependent on the external input. This introduces a paradigm shift in the field of reprogrammable mechanical metamaterial, allowing it to move from responsive to adaptive behaviour, where part of the state control is left to the metamaterial itself. The state-dependent switching behaviour of the unit cell was successfully analysed via FEA and validated by the fabrication and testing of a prototype. First simulations on potential metamaterial designs show promising results for emergent behaviour like adaptive property change, counting ability, and adaptive shape morphing. Even though the unit cell design was developed for sign-switching Poisson's ratio, the concept can easily be extended to facilitate other properties, for example, stiffness. Due to its monolithic and contactless 3D design, the developed unit cell is suitable for metamaterial tessellations at different length scales, e.g. microscale using two-photon lithography (Nanoscribe).

VI. Materials and Methods

Further details on the design can be found in Supplementary Material Section I. The method for the FEA is described in Supplementary Material Section II and the fabrication process is explained in Supplementary Material Section III. Procedures and observations from the experimental measurement are detailed in Supplementary Material Section IV. Additional results are presented in Supplementary Material Section V.

REFERENCES

[1] M. Kadic, G. W. Milton, M. Van Hecke, and M. Wegener, "3D Metamaterials," tech. rep.

[2] A. A. Zadpoor, "Mechanical meta-materials," 9 2016.

[3] T. A. Schaedler and W. B. Carter, "Architected Cellular Materials," 7 2016.

[4] K. Bertoldi, V. Vitelli, J. Christensen, and M. Van Hecke, "Flexible mechanical metamaterials," 10 2017.

[5] T. Chen, M. Pauly, and P. M. Reis, "A reprogrammable mechanical metamaterial with stable memory," *Nature*, vol. 589, pp. 386–390, 1 2021.

[6] N. Yang, C. W. Chen, J. Yang, and J. L. Silverberg, "Emergent reconfigurable mechanical metamaterial tessellations with an exponentially large number of discrete configurations," *Materials and Design*, vol. 196, 11 2020.

[7] A. Farzaneh, N. Pawar, C. M. Portela, and J. B. Hopkins, "Sequential metamaterials with alternating Poisson's ratios," *Nature Communications*, vol. 13, 12 2022.

[8] H. Yasuda and J. Yang, "Reentrant origami-based metamaterials with negative Poisson's ratio and bistability," *Physical Review Letters*, vol. 114, 5 2015.

[9] D. Restrepo, N. D. Mankame, and P. D. Zavattieri, "Phase transforming cellular materials," *Extreme Mechanics Letters*, vol. 4, pp. 52–60, 9 2015.

[10] C. Coulais, E. Teomy, K. De Reus, Y. Shokef, and M. Van Hecke, "Combinatorial design of textured mechanical metamaterials," *Nature*, vol. 535, pp. 529–532, 7 2016.

[11] J. R. Raney, N. Nadkarni, C. Daraio, D. M. Kochmann, J. A. Lewis, and K. Bertoldi, "Stable propagation of mechanical signals in soft media using stored elastic energy," *Proceedings of the National Academy of Sciences of the United States of America*, vol. 113, pp. 9722–9727, 8 2016.

[12] A. Ion, L. Wall, R. Kovacs, and P. Baudisch, "Digital mechanical metamaterials," in *Conference on Human Factors in Computing Systems - Proceedings*, vol. 2017-May, pp. 977–988, Association for Computing Machinery, 5 2017.

[13] T. Mei, Z. Meng, K. Zhao, and C. Q. Chen, "A mechanical metamaterial with reprogrammable logical functions," *Nature Communications*, vol. 12, 12 2021.

[14] L. J. Kwakernaak and M. van Hecke, "Counting and Sequential Information Processing in Mechanical Metamaterials," 2 2023.

[15] X. Ma and P. Yan, "Reprogrammable Mechanical Metamaterials with Heterogeneous Assembly of Soft Shell-Based Voxels," *Advanced Engineering Materials*, p. 2201323, 10 2022.

[16] S. Janbaz, K. Narooei, T. Van Manen, and A. A. Zadpoor, "Strain rate-dependent mechanical metamaterials," tech. rep., 2020.

[17] ten Wolde M. and Farhadi D., "A single input state switching building block harnessing internal instabilities," 6 2023.

[18] A. Walther, "Viewpoint: From Responsive to Adaptive and Interactive Materials and Materials Systems: A Roadmap," 5 2020.

[19] C. Kaspar, B. J. Ravoo, W. G. van der Wiel, S. V. Wegner, and W. H. Pernice, "The rise of intelligent matter," 6 2021.

[20] A. Numic, "Manipulating post-buckled compliant mechanisms Buckling mode interaction as a novel method of stiffness compensation," tech. rep., 2021.

Chapter 3

Supplementary Material: Unit Cell with Sign-switching Poisson's Ratio for Adaptive Mechanical Metamaterials

Unit Cell with Sign-switching Poisson's Ratio for Adaptive Mechanical Metamaterials

— Supplementary Material —

Luca Lagemann
Delft University of Technology
MSc Mechanical Engineering, High-Tech Engineering, Mechatronic System Design
Delft, Netherlands
l.lagemann@student.tudelft.nl

This document contains the following supplementary information:

CONTENTS

I. Design

This section provides an overview of design decisions, constraints, and derived knowledge that has influenced and led to the final design of the developed unit cell.

A. Design Decisions and Fixed Parameter

The general geometry of the developed unit cell is based on the well-known hexagonal honeycomb geometry. Two states are introduced by designing the side beams close to their bifurcation point, allowing the use of minimal geometric change to switch between conventional hexagonal shapes with positive Poisson's ratio and auxetic re-entrant hexagonal shape. An inclination angle of 1.4 degrees for the side beams turned out to provide sufficient state stability and deformation guidance while preserving small state transition displacements. The state transition strategy is adapted from a contactless single input state switching mechanism presented in [1].

The goal of this project was to introduce state-dependent switching combined with sign-switching Poisson's ratio as a material property into a unit cell design that can be tessellated to create 3D mechanical metamaterials. Design choices in the concept phase were guided by the aim of keeping the number of components and moving parts as small as possible. The two bistable elements (state element and non-linear spring) are orientated horizontally and connected to the thick horizontal frame beams to minimize influence on their bistable behaviour. Additionally, this setup allows to connect both frame sides to the same state element and non-linear spring. The central transmission mechanism connects the frame and bistable elements. Its rhombus shape introduces a leaver that can amplify forces or displacements in the system, based on its angle. This adds a simple parameter to tune the switching behaviour of the unit cell, which will be further elaborated in Section V.

The final design uses lumped compliance, where the deformations are concentrated in simple short-length flexures. Earlier versions with long-length flexures in the transmission mechanism turned out not to be manufacturable in a satisfactory quality with the chosen material and manufacturing process. Therefore the flexure design was limited to a minimum length and width of 5mm and 0.55mm respectively. Furthermore, the overall size was constrained by the build volume of the 3D printer, leading to a maximum height and width of 130mm for the unit cell frame dimensions. The width of the horizontal beams of the frame was set to 15mm to provide high rigidity within the given design space. For Finite Element Analysis (FEA) simulations of multiple connected unit cells, this value was increased to 22mm, since the width of 15mm still allowed neighbouring cells to influence the bistability and switching behaviour of the state element and non-linear spring. For better structural integrity the frame flexures were increased to a width of 0.65mm and length of 6mm.

Initial concepts of the unit cell were based on a 2D planar design which could have been manufactured by fused deposition modeling (FDM) 3D printing. However, these designs showed insufficient shear stiffness, leading to undesired lateral 'run-away' motion under compression. Moving from a 2D to a 3D design solved this issue since the out-of-plane stiffness of a single planar mechanism adds to the shear stiffness of the accompanying 90-degree rotated planar mechanism. The larger the frame thickness, the higher its shear stiffness. A thickness of 8mm was found to be sufficient. Additionally, going from a 2D to a 3D design is desirable for the creation of actual mechanical metamaterials.

B. Bistable Element Analysis

Since the unit cell functionality is highly dependent on the performance of the bistable elements, extended studies were carried out to analyse their behaviour and the effect of different design parameters. At first, Pseudo Rigid Body Modelling (PRBM) was used to create an analytical model of a simple bistable element by replacing the flexible short-length flexures of the compliant mechanism with an analogous rigid-body model, e.g. springs that store the energy introduced by deformations. [2] Torsional springs are used for the short-length flexures, while the axial compression stiffness is represented by a linear spring for each anchor point.

The energy stored in the two torsional springs and the linear spring is calculated using equations (1) and (2) respectively.

$$E_t = \frac{1}{2} K_t \theta^2 \tag{1}$$

$$E_l = \frac{1}{2} K_l {d_y}^2 \tag{2}$$

θ and d_y are functions of the input displacement u_x. The torsional stiffness K_t is defined by the dimensions of the short-length flexure, according to equation (3). The linear spring at the connection between flexure and frame provides a deterministic support stiffness, which is modelled as a fixed-fixed beam (anchor beam) with a concentrated central load, for this setting. The corresponding stiffness K_l is calculated with equation (4).

$$K_t = \frac{E t_f {w_f}^3}{12 l_f} \tag{3}$$

$$K_l = 192\frac{EI_a}{{l_a}^3} \tag{4}$$

I_a is dependent on the dimensions of the anchor beam, that provides the support stiffness. The sum of the potential energy terms is then differentiated with respect to the input displacement to derive the corresponding force-displacement behaviour.

$$F = \frac{\partial E}{\partial u} = \frac{\partial E}{\partial \theta}\left(\frac{\partial u}{\partial \theta}\right)^{-1} \tag{5}$$

Python was used to solve the equations and plot the resulting energy- and force-displacement graphs. The developed program also includes a graphical user interface (GUI) which allows to change individual design parameters via sliders. The corresponding energy and force plots are updated instantaneously. An additional function was implemented to export the current design parameter to a TXT file, which is linked to a Solidworks model that updates its geometry based on the values in the TXT file. The CAD model can then be saved as a STL file to 3D print the bistable element. Figure 1 demonstrates the concurrent workflow with screenshots of the GUI, exported design parameters, and the connected CAD model.

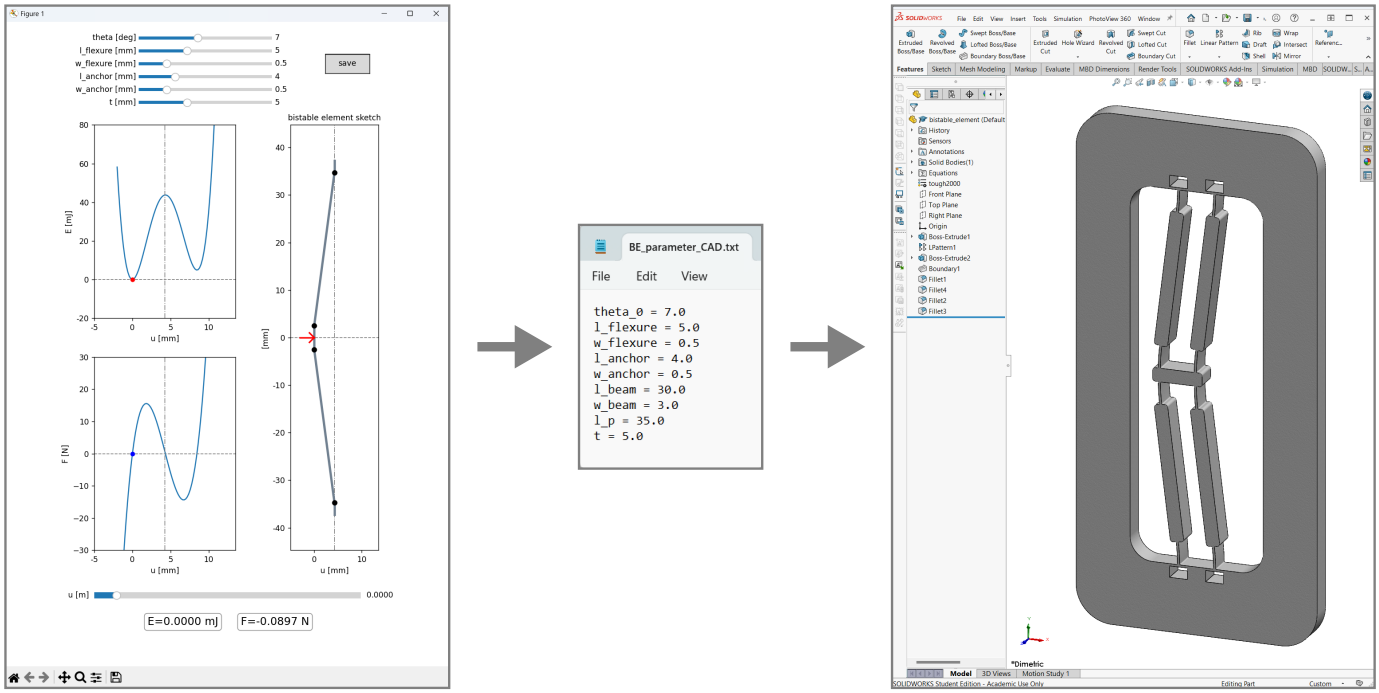

Fig. 1. Illustration of the bistable element development tool. The left image shows a screenshot of the GUI, which allows the user to manipulate the design parameters of the bistable element and investigate their influence on the strain energy and force-displacement curves. A button allows exporting the current set of design parameters to a TXT file, which is shown in the centre. This file is connected to a Solidworks CAD model, where the design of the bistable element is updated based on the values in the TXT file. The right image shows a screenshot of the generated CAD model in Solidworks.

This development tool provides valuable insights on the effect of individual design parameters on the behaviour of bistable elements, which helped to build a better understanding for later development stages of the project. A summary of the main influences and takeaways is given in Table 1. Note that the parameters were studied at a length scale suitable for FDM 3D printing. By dividing the parameter by the total length, for instance, one could convert the parameter influence to a scale-independent notion. Also, in this study, the width and length of the rigid beam sections were defined as 6 times the width and length of the flexures, according to a guideline from [3].
Even though PRBM is an effective method to model compliant mechanisms and gain insights to their deformation behaviour, it does not take stresses into account. The maximum allowable stress limits the performance of the bistable element. For example, large critical forces through high support stiffness or large initial angles are expected to be constrained by the stress limits. Therefore, FEA was used primarily for further development of the unit cell.

C. Design Criteria

Based on the defined frame dimensions described above, it was decided that the lateral displacement of the frame side midpoints upon state transition (d_x) should be minimum twice the initial distance to the bifurcation point (vertical axis). Therefore, d_x should be at least 2.015mm. This is not necessarily a hard requirement but keeping the displacement above this value ensures

TABLE I
DESIGN PARAMETERS OF THE INVESTIGATED BISTABLE ELEMENT AND THEIR INFLUENCE.

parameter	**influence & take-away**
theta	A larger initial angle of the bistable element increase the central potential energy peak and therefore the critical forces. It also increases the travel distance. This parameter can be used to increase the bistability without changing the overall length of the bistable element, which can be valuable in a limited design space.
flexure length	Since the flexure length was coupled to the overall length, its increase results in a larger travel distance and larger overall dimensions of the bistable element. Very small flexure lengths e.g. lower than 2mm lead to monostability.
flexure width	The width of the flexure has a large effect on the 2nd stable point since the strain energy is directly proportional to the cube of the flexure width. Thick flexures, e.g. >1.3mm, lead to monostability. Ideally, the potential energy in both stable points is the same, to have equally stable states with the same critical forces. Hence, the flexures should be as thin as possible.
anchor length	Increasing the length of the anchor beam lowers the support stiffness. As a result, the energy barrier between the two states is lowered and therefore also the critical forces. Insufficient support stiffness results in monostability. The maximum length of the anchor beam might be constrained by the general design and structural arrangement of the bistable element.
anchor width	Similar to its length, the anchor width defines the support stiffness. Here a thinner anchor decreases the bistability. Both parameters influence the strain energy by a factor of its cube. Thus, it is valid to fix one of the two parameters while tuning the other.
thickness	The out-of-plane thickness of the bistable element can also be used to tune the bistability. In contrast to the anchor dimensions, the thickness also influences the torsional stiffness of the flexures and therefore affects the energy of the second stable position. By changing the thickness the critical forces can be scaled, without changing the in-plane geometric layout of the bistable element.

state stability. If d_x is insufficient, the unit cell would not be able to enter its second, re-entrant state. The parameter study in Section V shows the consequence of lower d_x values.

In order to achieve the specified d_x, the transmission mechanism needs to be stretched vertically by a certain displacement d_y and force F_y, as shown in the sketch in Figure 2A. Note that the displacements are exaggerated for better visualization. The rhombus-shaped transmission mechanism can serve as a lever, which amplifies forces or displacements in the system, depending on its initial angle α_0. FEA was used to determine the required d_y and F_y for different α_0. Figure 2B shows the result of this analysis by plotting required d_y and F_y over the lateral displacement of the frame sides d_x.

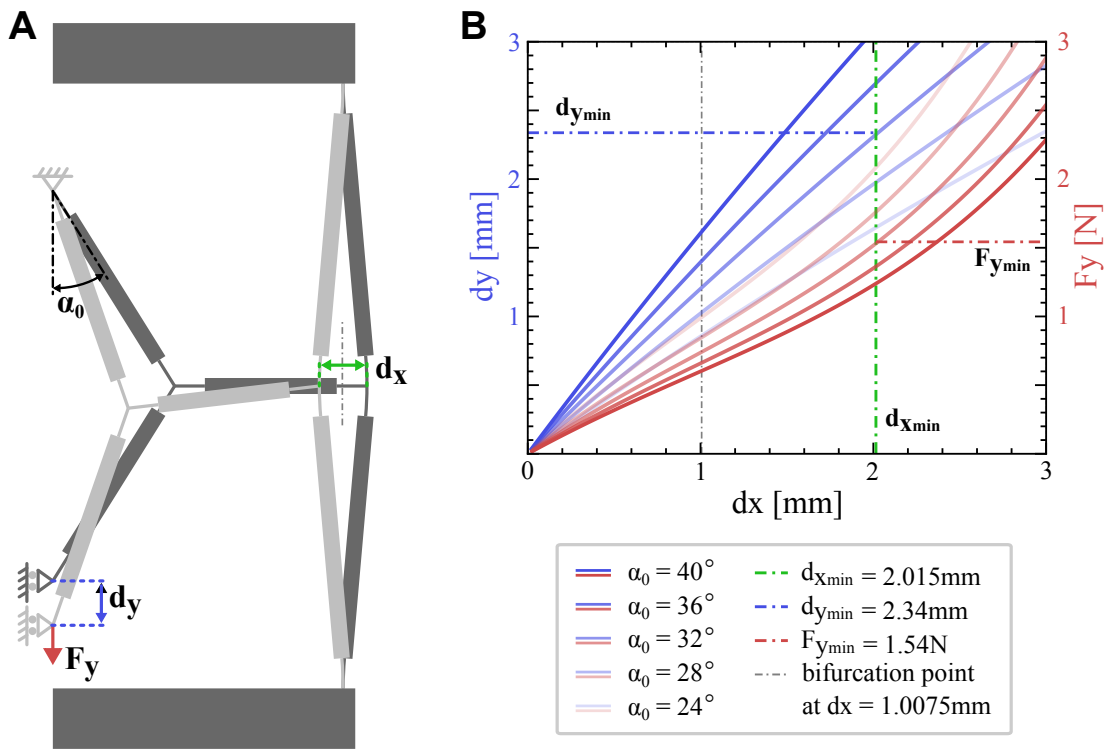

Fig. 2. Required internal force and displacements to achieve the two desired unit cell states. **A** shows a sketch of the right half of the unit cell in its two states, pointing out the force and displacement, by which the central transmission mechanism needs to be stretched vertically to pull the frame sides to the second state configuration. The hexagonal shape with positive Poisson's ratio is shown in dark grey and the re-entrant, auxetix state is shown in light grey. **B** graphs the vertical force and displacement over the lateral displacement of the frame sides for a range of initial rhombus angles α_0. The required minimum values for the selected angle of 32 degrees and a minimum lateral displacement d_x are given in the legend and highlighted in the plot.

As shown in Figure 2B, small rhombus angles require a lower d_y and larger F_y, while larger angles require larger d_y and

lower F_y. Since d_y is linked to the displacement difference between the state element and non-linear spring, and F_y needs to be generated by the second state of the non-linear spring, it is desired to keep both values relatively low. It was decided to use a rhombus angle of 32 degrees since it represents a good balance between required force and displacement. As a result, the minimum vertical force was set to F_{ymin} = 1.54N and the minimum vertical displacement was set to d_{ymin} = 2.34mm. These values were used in combination with parametric studies to find suitable state element and non-linear spring designs, which will be discussed in the following section.
Another important design criterion to ensure proper functionality of the unit cell is that the second critical force of the state element (F_{s2}) is sufficiently larger than the first critical force of the non-linear spring (F_{n1}). If this is not the case, the state element switches back to its initial state, before the non-linear spring switches, leaving the re-entrant unit cell state inaccessible. To prevent this, it was decided to find a combination of state element and non-linear spring that has a safety margin of minimum 1N between F_{s2} and F_{n1}.

D. State Element & Non-linear Spring Parametric Study

Manual parameter adjustments to tune the bistability of the state element and non-linear spring are time-consuming and insufficient in order to find a working combination that fulfils the desired global deformation behaviour. Therefore, a parametric study was conducted on selected design parameters of the state element and non-linear spring. Although the PRB analysis showed that the length and width of the flexures present an important parameter (see Table 1), their values are limited by the manufacturing process. Additionally, the length of the anchors was defined as a function of θ and l to ensure a sufficient gap and avoid contact between the horizontal frame beams and the bistable element. The thickness of the bistable element was set to be 6mm for the state element since a larger thickness allows to generate high forces at small displacement, which is desired for the state element. For the non-linear spring the opposite is needed: smaller forces at larger displacements, which can be provided by a lower thickness, e.g. 3mm. Table 2 gives an overview of the parameter design space used for the parametric study, which was defined based on gained knowledge from the PRBM and manufacturing limitations.

TABLE II
PARAMETER SPACE FOR THE PARAMETRIC STUDY OF THE STATE ELEMENT AND NON-LINEAR SPRING.

	design parameter space						
	θ [deg]	l [mm]	wa [mm]	la [mm]	wf [mm]	lf [mm]	t [mm]
state element	5 - 8	20 - 34	3 - 5	l*sin(θ)+3.5	0.55	5	6
non-linear spring	5 - 8	34 - 48	3 - 5	l*sin(θ)+5	0.55	5	3

FEA was used to model the two bistable elements and derive their force-displacement characteristics as well as maximum stresses. The results were then filtered based on their critical forces, displacements, and maximum stress. For the state element, the parametric study was used to identify a design that is within the stress limit of 39MPa and facilitates reasonable high forces at small displacements. The stress limit is derived from the tensile strength of the material and a safety factor of 0.85 [4]. Furthermore, it is desirable to keep the absolute value of the two critical forces as close as possible to achieve similar switching forces. With these criteria in mind, a set of design parameters was chosen from the results of the parametric study. The left side of Figure 3 shows the force-displacement graph of the selected state element in contrast to other parameter combinations from the parametric study. Designs that violate the stress constraint are shaded in red. The star markers point out relevant characteristics that are used for the definition of the non-linear spring design. The right side of Figure 3 presents the corresponding values and selected design parameters.
With a defined state element, potential non-linear spring designs can be identified by filtering the results of its parametric study based on certain design criteria, as described above. The filters are defined as follows:

1) $\sigma_{max} < 39$ MPa,
2) $F_{n1} < F_{s2}$ -1N
3) $F_{n2} < F_{ymin}$
4) $d_s + d_y +$ 0.25mm $< d_{n2} < d_s + d_y +$ 0.25 mm

The left side of Figure 4 visualizes how the filters have been applied to the results of the non-linear spring parametric study. Note that the force-displacement curve of the state element (dashed line) is plotted with inverted force values for better referencing of the criteria.
The remaining coloured force-displacement curves in Figure 4 represent potential non-linear spring designs that fulfil the specified criteria. Based on these parameter combinations, the non-linear spring design parameters were defined as shown on the right of Figure 4.

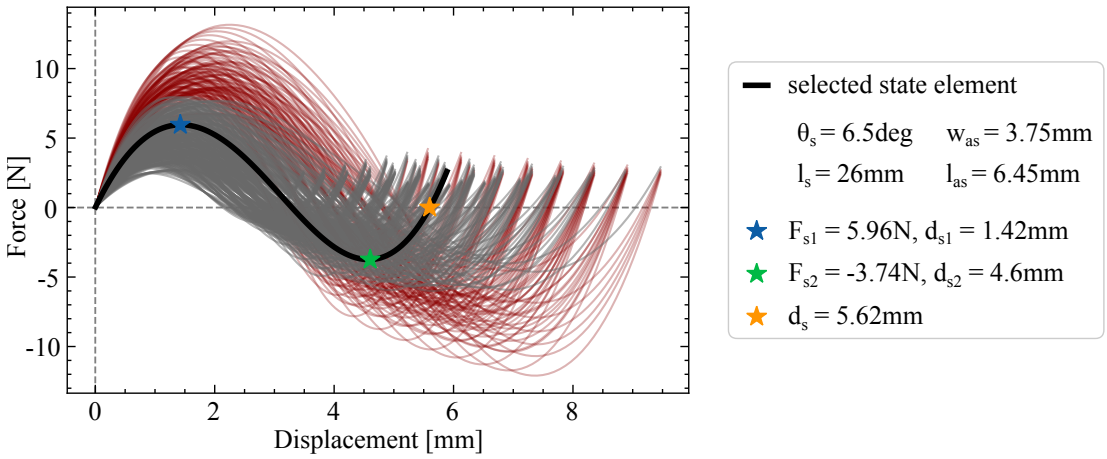

Fig. 3. Results from the parametric study of the state element, showing the force-displacement curve of the selected state element design (thick black line) compared to all other parameter combinations. The red curves represent designs that violate the stress limit. The legend on the right summarizes the design parameter of the selected state element and its key characteristics.

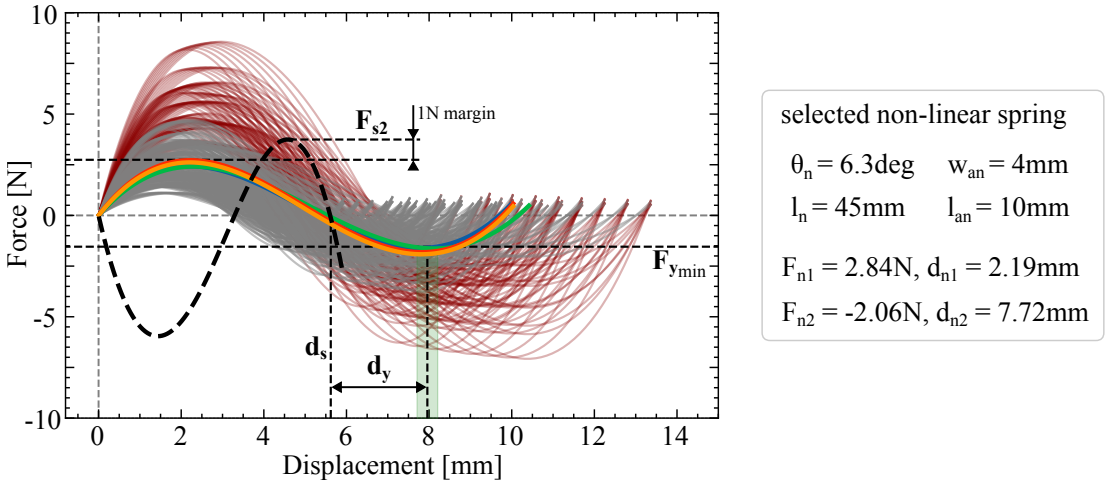

Fig. 4. Results from the parametric study of the non-linear spring and the applied filter according to the specified criteria. The selected state element design (dashed line) is plotted with inverted force to highlight the force requirement between F_{s2} and F_{n1}. Red curves represent design combinations that violate the stress constraint. The green zone represents the displacement range in which F_{n2} should be. The right side of the figure presents the design parameter and important characteristics of the selected non-linear spring design.

The parametric studies were an effective tool to drastically reduce the large number of parameter combinations to a few suitable designs, based on which the final design was selected. It is important to note, that the parametric study was not conducted to find the optimal design but rather to narrow down the large design space based on certain criteria. Also the defined criteria are not necessarily hard constraints. For example, it was decided that d_x should be 2.015mm to have hexagonal and re-entrant unit cell states of equal initial angle. For other frame designs or state requirements this value will vary, leading to different criteria values and therefore other state element and non-linear spring designs. However, the design selection process is still applicable.

II. Finite Element Analysis

ANSYS mechanical APDL was used as the FEA software due to its parametric programming language and customizability. The FEA models were set up based on a static, non-linear analysis with a linear elastic material model and 2.2GPa as Young's modulus. Two node beam elements according to Timoschenkov beam theory (BEAM188) were used in combination with parameterized key-point coordinates to model the 3D structure. A mesh sensitivity analysis was carried out to determine the number of elements per beam. All flexure and anchor beams were divided into 15 sections along their length and received 6 and 2 cells along their width and thickness respectively. The stiffer beams, which are not expected to undergo any significant bending, are divided into 5 sections with single-cell cross sections. The horizontal frame beams are modelled with 8mm long elements and a 2x2 cell cross section.

To create metamaterial structures, *DO loops and the LTRAN command were used to pattern the unit cell. Neighbouring cells were then connected using the CPCYC command for offset nodes and CPINTF for coincident nodes. The developed script

allows to generate 3D metamaterial structures based on the number of cells in the x-, y-, and, z-direction specified at the beginning of the script.
For the analysis of a single unit cell, the bottom central node is fixed by constraining all of its six degrees of freedom, while a vertical input displacement is applied to the top central node. In the case of multiple connected unit cells, one bottom cell is fully constrained whereas the remaining bottom cells are free to move in plane (x-z) and the input displacement is applied to all top cells. Figure 5 shows an element plot of the modelled structures and the applied boundary conditions.

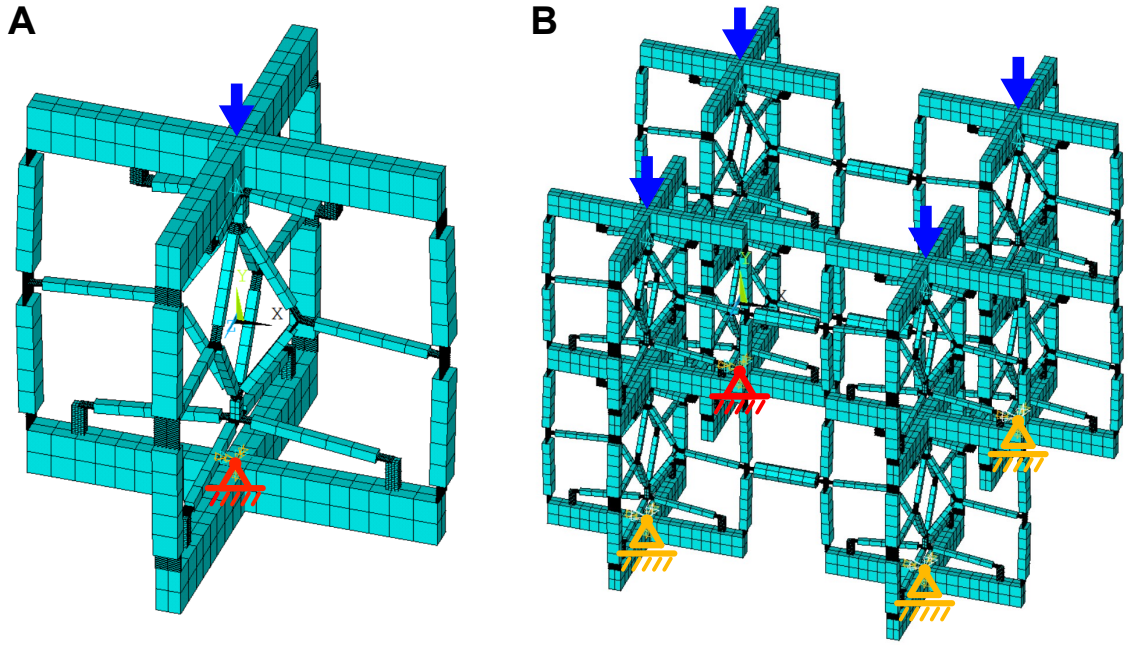

Fig. 5. Element plot of the FEA and the applied boundary conditions. **A** shows the FEA model of the single unit cell with a fixed bottom central node, as indicated in red, and a vertical input displacement (blue arrow) at the top central node. **B** shows the FEA model of the 2x2x2 tessellation, where one of the bottom cells has a fixed central node and the other three bottom cells are free to move in the x-z plane. The input displacement is applied to all four top cells.

Six load steps are used in the simulation to analyse the deformations of the unit cell under two consecutive loading cycles. In the first and second steps, a ramped input displacement of 1.5mm was applied and removed respectively. Load step 3 is used to remove all inputs and let the structure settle. The same procedure is applied in steps 4, 5, and 6 which represents the second loading cycle. Finally, the sparse solver is used and the time step size was tuned for individual simulations. Animations of the deformations over the six load steps can be found in the repository under the link provided in Section S6.
The results of the simulation were first inspected in the ANSYS software and then exported to TXT files for further analysis in Python, especially in the cases of parametric studies.

III. Fabrication

For experimental validation, a unit cell prototype was fabricated through stereolithography (SLA) on a Formlabs Form 3 printer. Figure 6 provides a summary of the fabrication steps. The material Tough2000 was chosen due to its high ratio between tensile strength and Young's modulus, compared to other available materials [4]. A high tensile strength and low Young's modulus allows to achieve larger displacements before the stress limit is reached, which is desirable for compliant mechanisms.
A CAD model of the unit cell was designed in Solidworks and prepared for printing using Formlabs 'Preform' software. As shown in Figure 6A, the unit cell was oriented horizontally to achieve the best print quality. Earlier test prints in upright orientation showed sagging of the flexures, which had a negative influence on the bistability. The layer height was set to 0.1mm and the touchpoints for the support structure were defined manually. The model took 11 hours and 13 minutes to print and used 175ml of the print material. Figure 6B shows the structure after the printing process has just finished. A flexible build platform was used to make the removal of the print easier.
Post-processing of the print was done according to the equipment manufacturer's recommendation: two times 10 minutes washing in IPA using the 'Form Wash' machine and 60 minutes curing at 70 degrees Celsius in the 'Form Cure' machine. It is important to let the part dry completely before starting the curing process to minimize warping. Compressed air was used to speed up this process. Finally, the support structure was removed using tweezers and a wire cutter. The final prototype is shown in Figure 6D.

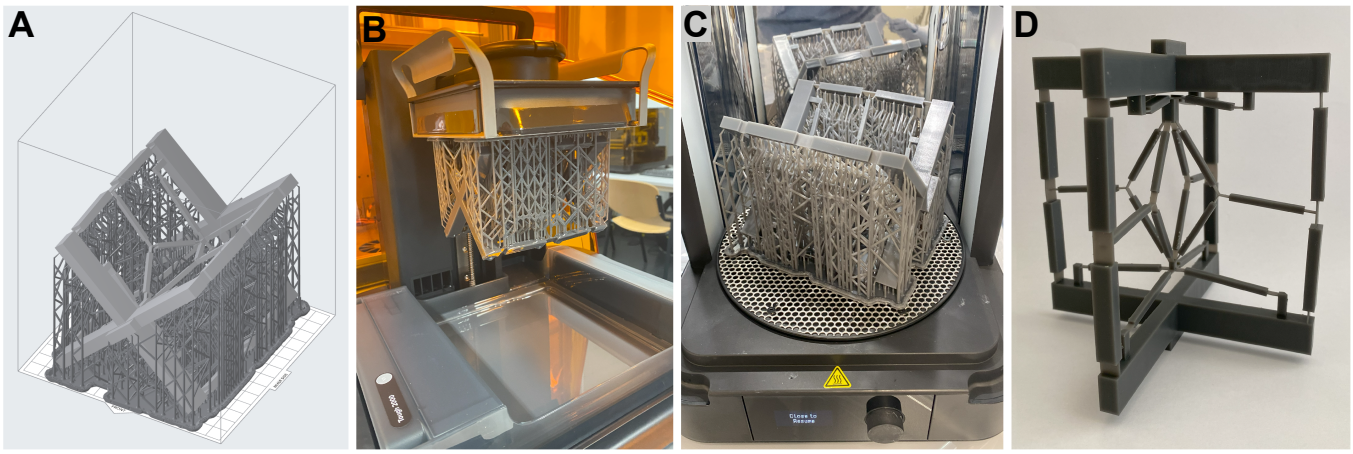

Fig. 6. Fabrication process of the unit cell prototype. **A** Screenshot of the 3D model in the slicer software 'PreForm', where the print settings and support structure are defined. **B** Photo of the just finished print inside the Formlabs Form 3 printer. **C** The printed structure inside the 'Form Cure' curing machine, where it is cured for 60 minutes at 70 degrees Celsius after it has been washed in IPA twice for 10 minutes. **D** The final unit cell prototype, after the support structure has been removed.

IV. Experimental Measurement

For experimental validation, the prototype was tested in a tensile test machine (Zwick Roell Z005) to analyse the force-displacement characteristic. Figure 7 shows the measurement setup in A and a close-up photo of the mounted prototype in B. The prototype was clamped at both ends via tabs that were implemented in the design for this purpose (see also Figure 6D). Red markers were placed on the prototype and filmed during the experiment. The video material was later analysed using image processing to determine the lateral displacement.

The input displacement was applied at a fixed rate of 10mm/min and one minute pause between each loading cycle. The pause was used to save the data from each run because the software was prone to crash unexpectedly, which led to data loss. A total of 28 loading cycles were performed, of which 14 were recorded on camera for displacement tracking. A video of two consecutive displacement cycles is available in the repository, linked in Section 6. Experiments on individual bistable elements were done using a linear stage (PI M505) with a 45N force sensor (Futek LSB200 FSH03875).

Fig. 7. Experimental measurement. **A** Overview of the measurement setup, showing the tensile test machine on the right and the computer with the operating test software on the left. **B** Close-up photo of the clamped unit cell prototype, showing the markers that were placed for displacement tracking.

A. Data Processing

The force-displacement data from the experimental measurement was exported as a TRA file from the tensile test machine. To evaluate the lateral deformation of the unit cell, markers in the form of red stickers were placed on the prototype. The deformation was recorded using a camera (iPhone 11 Pro) mounted on a tripod. The recordings were triggered via a Bluetooth remote control to avoid camera movement. An available Matlab script was used to convert the video frames to binary images, based on a colour threshold of the markers. The location of the centroids of the isolated marker is then tracked for each

frame and converted to millimetre scale with a previously determined pixel-to-millimetre ratio. The resulting displacements in form of coordinates were then exported as a TXT file. Python was used to further process and to calculate the mean of the force-displacement data from the tensile machine and the tracked displacements from the videos.

B. Viscoelastic Behaviour

The experimental measurement has shown non-linear material behaviour in the form of viscoelasticity. The hysteresis in the force-displacement plots indicates that energy is dissipated due to the damping capacity of the material. Experiments on individual bistable elements using the same fabrication process support this hypothesis. Figure 8 shows the force-displacement results of a bistable element at two different actuation speeds and compared to the FEA result. The results clearly show that the actuation speed has an influence on the force profile caused by the viscoelastic property of the material.
Furthermore, the test object was held at both endpoints (zero and full displacement) for two minutes. During this time the force decreased as can be seen in the force displacement graph in Figure 8B, highlighting the effect of stress relaxation. Interestingly, the absolute value of the second critical force is increased as a result form the stress relaxation. Thereby the ratio between the two critical forces is closer to 1, which can be beneficial for the functionality of the unit cell.
The hysteresis in this experiment is caused by both the energy dissipation of the material and compliance in the measurement setup. To eliminate the effect of the unknown stiffness introduced by this measurement setup, the full unit cell was tested on the Zwick Roell tensile test machine.

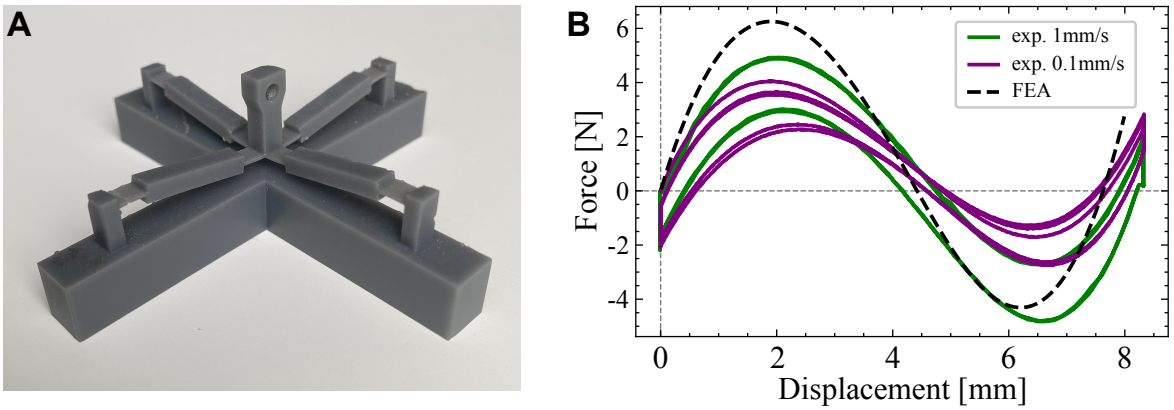

Fig. 8. Experimental measurement of a single bistable element. **A** Photo of the fabricated and tested bistable element. **B** Force-displacement results from the measurement at two different actuation speeds and compared to the FEA results, demonstrating the effect of vicoelasticity on the critical forces.

V. Additional Results

This section contains additional results on unit cell level, that demonstrate the effect of individual design parameters on its performance. Furthermore, other metamaterial designs are presented and investigated.

A. Unit Cell Parameter Influence and Tunability

An FEA model of the full unit cell design was used to analyse the effect of individual design parameters on the overall unit cell behaviour. In this analysis, the width of the horizontal frame beams was increased to 25mm for increased state stability. The initial rhombus angle α_0 was varied for the range from 26 to 38 degrees in steps of 2 degrees. In another study values from 36 to 48mm in steps of 2mm were used for the length of the non-linear spring (l_n). Figure 9 A and C show the resulting input-output displacement relation for the different values of l_n and α_0 respectively. The corresponding force-displacement plots are shown in B and D. The line opacity of the graph is decreased with the value of the varied design parameter. The color green indicates that the unit cell is in the hexagonal state with positive Poisson's ratio and the auxetic re-entrant state is highlighted in red.
The results show that a larger rhombus angle results in larger switching forces and smaller switching displacements for both unit cell states, while smaller α_0 values have the opposite effect. The length of the non-linear spring on the other hand only has an effect on the switching behaviour of the negative Poisson's ratio state. Here a larger value of l_n causes delayed switching and lower forces. Furthermore, the non-linear spring length effects the lateral distance (d_x) between the two stable states of the unit cell at zero axial input displacement, whereas the rhombus angle shows no influence on d_x. The smallest value of l_n (36mm) in fact resulted in an insufficient d_x which did not allow the unit cell to enter its second (re-entrant) state, as can be seen in plot A of Figure 9, where the displacement curve of lowest opacity returns to positive lateral displacement even for the second state.

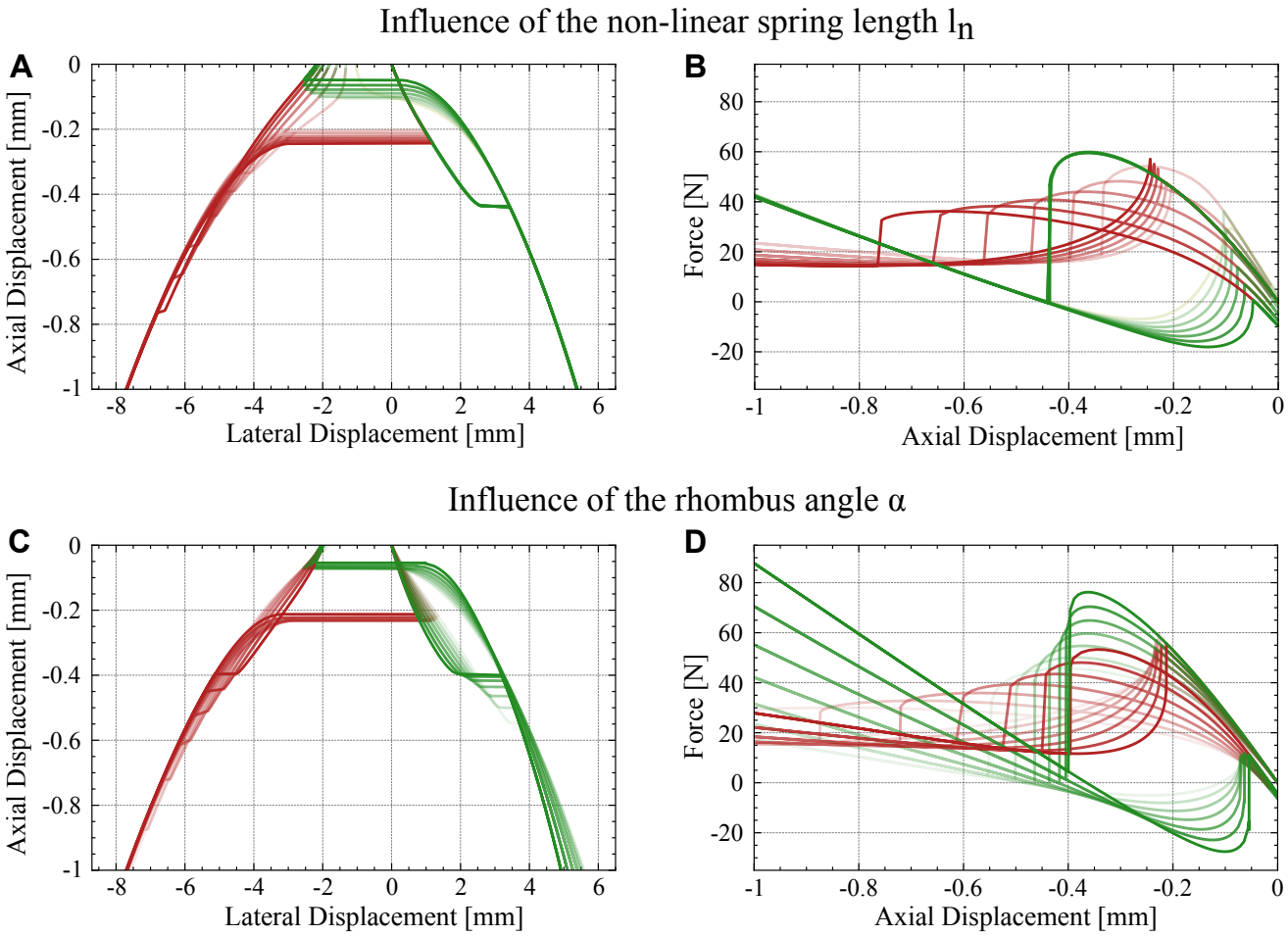

Fig. 9. Results from the unit cell FEA parameter analysis. The effect of the non-linear spring length l_n is shown in **A** and **B**, whereas **C** and **D** highlight the influence of the rhombus angle α_0. The values for l_n range from 36mm to 48mm and the for α from 26 degrees to 38 degrees. The line opacity is decreased with the value of the design parameter. Loading cycles in the positive and negative Poisson's ratio state are plotted in green and red respectively.

This parametric study highlights the effect of the initial rhombus angle and the length of the non-linear spring on the unit cell level. Both represent an effective parameter to tune the the performance of the unit cell, especially the rhombus angle since it does not compromise d_x and therefore the state stability of the unit cell.

B. Adaptive Shape Morphing

The sign-switching Poisson's ratio of the unit cells can also be used in a tessellated structure to achieve shape morphing similar to what has been demonstrated by active mechanical metamaterial example in [5]. State-dependent switching introduces a degree autonomy where the unit cell changes state if it needs to, which can be used as a form of learning ability. To demonstrate this, two columns of three unit cells are connected in parallel by a horizontal link between their frame sides, as shown in Figure 10.

Initially all unit cells are in their hexagonal state with positive poissons ratio (Figure 10A). An input displacement of 0.8mm is applied (grey arrows) causes the metamaterial to expand laterally. The resulting planar shape is indicated by the grey dotted lines in Figure 10A'. Since the no state switching occurred, the metamaterial remains in the same initial configuration, when the input is removed, as shown in Figure 10B. Now, if a higher input displacement, in this case 2mm (black arrows), is applied and the lateral displacement is constrained in certain places, a few unit cells undergo state change. The pink star marker in Figure 10E points out which state elements have switched. As a result, the metamaterial has a new initial configuration, where some unit cells have switched to their second, re-entrant state. The colour contour in c highlights those cells by tracking their vertical displacement caused by the state change of the state element. In this configuration the same input displacement from A' causes the metamaterial to express the deformation behaviour it has 'learned' in the previous loading cycle, even when the boundary conditions are removed. In this case, the metamaterial morphs into a sinusoidal shape, as indicated by the grey dotted lines in C'. This deformation behaviour remains, until the switching threshold of individual unit cells is surpassed by a set of different boundary- and loading conditions. This behaviour demonstrates the ability of the metamaterial to adapt its

shape to varying external conditions, based on the input displacement and internal state information, which could be seen as a form of associative learning [6].
Note that the colour contours in Figure 10 are used to demonstrate the deformation behaviour qualitatively rather than quantitatively. Therefore, no specific values are presented for the colour map.

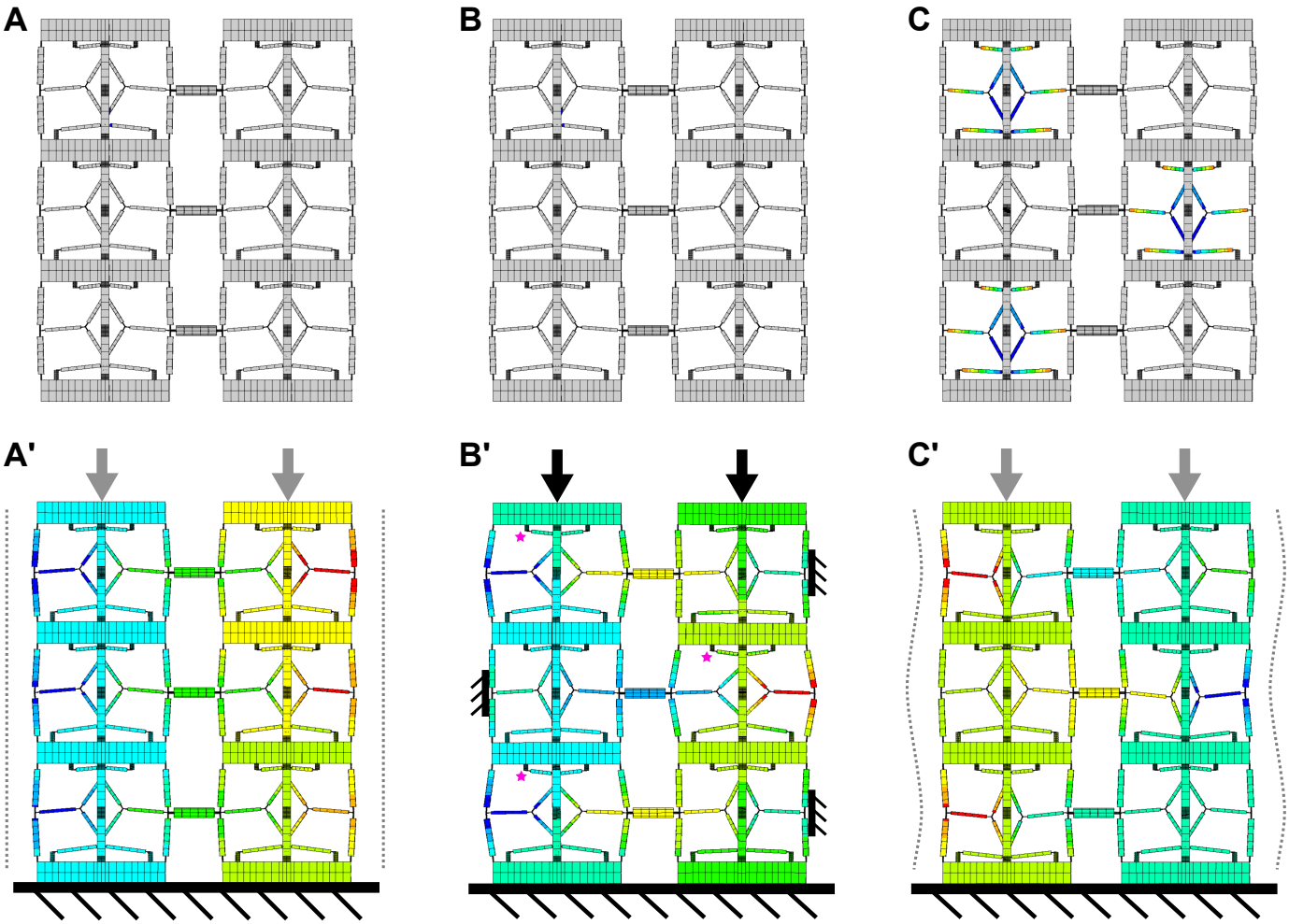

Fig. 10. Displacement characteristic of the 2x1x3 unit cell tessellation under different boundary conditions, highlighting its adaptive shape morphing capability. Sub-figures **A** to **C** show the metamaterial in its stable configuration without any loads applied (ground state). The colour contour for these figures graphs the vertical displacement to indicate state change of individual unit cells. **A'** to **C'** show the deformation of the equivalent initial configuration under certain boundary conditions and input displacements (arrows and black bars). Here the color contour shows the lateral displacement of the structure to point out the shape-morphing characteristic. Initially, all unit cells are in their hexagonal state with positive Poisson's ratio (**A**), leading to homogeneous expansion of the metamaterial, as displayed in **A'**. In **B** special boundary conditions are applied, which cause some unit cells to switch states under the applied input displacement. The new stable configuration and its deformation behaviour are shown in **C** and **C'** respectively.

C. Honeycomb Tessellation

Another interesting approach to create a metamaterial from the developed unit cell would be to use a tessellation similar to a honeycomb structure. In this case, additional unit cells are implemented in the empty centre of four neighbouring cells (2x2), as shown in the image of modelled structure in Figure 11. This tessellation is expected to promote simultaneous switching since unit cell frame sides are shared and rows of cells are not isolated. Therefore, if one cell switches, its neighbours should switch as well, causing a chain reaction throughout the metamaterial. This could be used for signal transmission similar to [7] but where the same input can be used for transmission and resetting. Furthermore, this type of tessellation could help to compensate for the low post-switching stiffness of the re-entrant unit cell state by prohibiting shearing between unit cell layers. Even though the structure was successfully modelled in FEA, no full investigation on this type of tessellation could be performed since the simulation was slow and struggled to converge past the first loading cycle. Therefore, further investigation is needed to explore its potential.

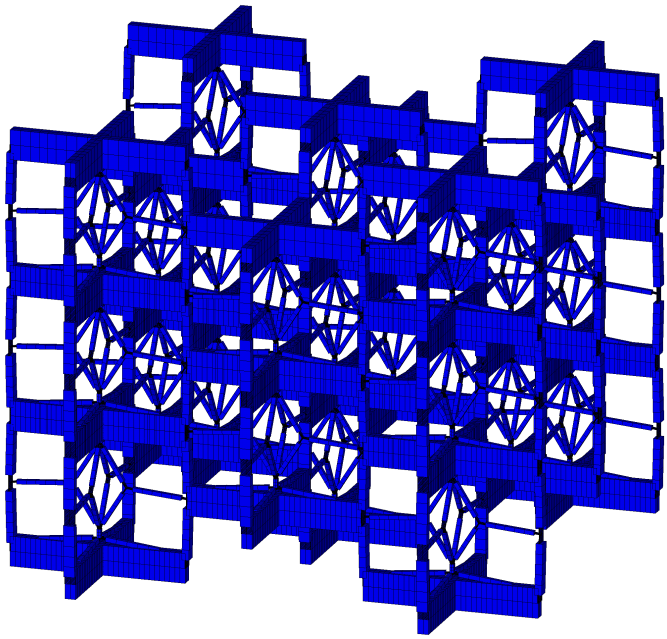

Fig. 11. Structural representation of a type of honeycomb tessellation, where intermediate unit cells are implemented to connect parallel columns of unit cells and bridge previously independent rows of cells.

VI. Data Availability

All files, data, and figures used in this project are available in the following GitHub repository. For the time the embargo is in place, only supporting videos are publicly accessible.

https://github.com/luca1579/MastersThesisLuca

References

[1] ten Wolde M. and Farhadi D., "A single input state switching building block harnessing internal instabilities," 6 2023.
[2] L. Howell, "Compliant_Mechanisms," *Wiley*, 2001.
[3] JPE, *Precision Point*. fourth ed., 2019.
[4] formlabs, "Materials Library," 2022.
[5] S. Thomas and J. Lipton, "Reprogrammable Surfaces Through Star Graph Metamaterials," tech. rep.
[6] A. Walther, "Viewpoint: From Responsive to Adaptive and Interactive Materials and Materials Systems: A Roadmap," 5 2020.
[7] J. R. Raney, N. Nadkarni, C. Daraio, D. M. Kochmann, J. A. Lewis, and K. Bertoldi, "Stable propagation of mechanical signals in soft media using stored elastic energy," *Proceedings of the National Academy of Sciences of the United States of America*, vol. 113, pp. 9722–9727, 8 2016.